Geo-Marine Letters
2020, Volume 40, Pages 507-523
https://doi.org/10.1007/s00367-019-00635-6
https://archimer.ifremer.fr/doc/00610/72215/

Archimer
https://archimer.ifremer.fr

Foraminiferal $\delta^{18}O$ reveals gas hydrate dissociation in Arctic and North Atlantic ocean sediments

Dessandier Pierre-Antoine [1, *] , Borrelli Chiara [1, 2], Yao Haoyi [1], Sauer Simone [1, 3], Hong Wei-Li [1, 4], Panieri Giuliana

[1] Department of Geosciences, CAGE–Centre for Arctic Gas Hydrate, Environment and Climate, UiT The Arctic University of Norway in Tromsø, Tromso, Norway
[2] Department of Earth and Environmental Sciences, University of Rochester, Rochester, NY, USA
[3] IFREMER-Institut Français de Recherche pour l'Exploitation de la Mer, Plouzane, France
[4] Geological Survey of Norway, Trondheim, Norway

* Corresponding author : Pierre-Antoine Dessandier, email address : pierre-antoine.dessandier@uit.no

Abstract :

Paleoceanographic investigations in the Arctic and north Atlantic are crucial to understanding past and current climate change, in particular considering amounts of pressure-temperature sensitive gas stored in marine sediments of the region. Many paleoceanographic studies are based on foraminiferal oxygen and carbon stable isotope compositions (δ18O, δ13C) from either planktonic specimens, benthic specimens or both. However, in seafloor regions promixal to high upward methane fluxes, such as where seafloor gas emission and shallow gas hydrate-bearing sediment occur, foraminiferal δ18O and δ13C display a wide range of values. Our study focuses on foraminiferal stable isotope signatures in shallow sediment at core sites in the Arctic and North Atlantic affected by significant upward flow of methane. This includes cores with shallow sulfate methane transitions that are adjacent to seeps and containing gas hydrate. We place emphasis on potential effects due to gas hydrate dissociation and diagenesis. Gas hydrate dissociation is known to increase pore-water δ18O, but our results indicate that precipitation of methane-derived authigenic carbonate (MDAC) also affects the foraminiferal δ18O of both planktonic and benthic species. In addition to this post-depositional overprint, we investigate the potential bias of the stable isotope record due to ontogenetic effects. Our data show that the size fraction does not impact the isotopic signal of planktonic and benthic foraminifera.

Please note that this is an author-produced PDF of an article accepted for publication following peer review. The definitive publisher-authenticated version is available on the publisher Web site.

1. Introduction

The Arctic is particulary sensitive to climate change (e.g., IPCC13; Screen and Simmonds, 2010; Serreze and Barry, 2011) and mulltiple oceanographic parameters are rapidily changing (Jakobsson et al., 2008). The Arctic is a fundamental component of the climate system because of its role in global carbon cycling (e.g., McGuire et al., 2009). First, the Arctic Ocean sequesters carbon dioxide that enters North Atlantic Deep Water. Second, the Arctic modulates carbon exchange with the atmosphere because of seasonal sea-ice coverage (e.g., McGuire et al., 2009). Third, the region contains very large amounts of methane in permafrost and gas hydrates, both which are sensitive to temperature change (Corell et al., 2008).

Along the Arctic continental shelves and slopes, probably between 30 and 170 Pg of methane exists as gas hydrate (e.g., Kvendvolden 1988; McGuire et al., 2009; James et al., 2016). Gas hydrates are crystalline solids that consist of gas (mostly methane) trapped in a lattice of hydrogen-bonded water molecules (Sloan and Koh, 2007). Hydrates are stable at relatively low (< 10°C) temperatures and moderate (>3-5 MPa) pressures, which at high latitudes generally correspond to water depths greater than 300 m (James et al., 2016). However, warming of intermediate- and deep-water masses or depressurization because of isostatic rebound might trigger hydrate dissociation (Thomas et al., 2002; Yao et al., 2019). Already, it has been estimated that dissociation of gas hydrates located on Arctic shelves contributes 0.08-0.13 Tg of methane per year to the atmosphere (McGuire et al., 2009).

Methane in marine sediment is significantly depleted in ^{13}C, often having a stable carbon isotope composition ($\delta^{13}C$) less than <-40 ‰ (Whiticar, 1999). In areas characterized by upward methane seepage, consumption of this methane by aerobic and anaerobic processes and the stable carbon isotope composition ($\delta^{13}C$) of DIC in bootom water and especially pore water and can become greately depleted in ^{12}C. Benthic foraminifera living on or just below the seafloor precipitate carbonate shells (or tests) using ambient dissolved inorganic carbon (DIC) (McCorkle et al., 1990). Benthic foraminifera have been widely used to reconstruct methane seepage at cold seeps andb gas hydrate-rich sediments (e.g., Wefer et al., 1994; Kennett et al., 2000; Hill et al., 2003; Barbieri and Panieri, 2004; Martin et al., 2007 and 2010, Panieri et al., 2009, 2012, 2014 and 2016; Consolaro et al., 2015; Schneider et al., 2018). However, it has been demonstrated that both benthic and planktonic foraminifera can be affected by diagenetic processes, particularly the secondary overgrowth precipitation of methane derived authigenic carbonate (MDAC). While it is now accepted that MDAC

overgrowth alters the $\delta^{13}C$ of the formainiferal isotope record (Torres et al., 2003; Panieri et al., 2016, 2017a; Schneider et al., 2017 and 2018; Consolaro et al., 2018; Wan et al., 2018), the impact of such diagenesis on foraminiferal $\delta^{18}O$ is less clear. In studies involving hydrate stability reconstructions, both the stratigraphy and climate variations are usually interpreted basd on the foraminiferal d18O record (e.g., Dickens et al., 1995; Kenett et al., 2000; Thomas et al., 2002). Nevertheless, the climate reconstruction approach is problematic in cold seeps releasing methane from gas hydrate source, as one would expect considering that the water trapped in gas hydrates is more enriched in ^{18}O compared to the adjacent pore water (Davidson, 1983). During gas hydrate dissociation, ^{18}O-enriched water is released, and this signal can potentially be incorporated in the shell precipitated by living benthic foraminifera. In addition, this signal can be captured by the MDAC precipitating on the foraminiferal shell after the death of the organisms (secondary overgrowth).

In this study, we investigate living and fossil foraminiferal specimens from different cold seeps in the Arctic Ocean and the Norwegian Sea to understand if and how methane release and/or hydrate dissociation can affect the foraminiferal $\delta^{18}O$ signature. We generate new foraminiferal $\delta^{18}O$ data sets using living (Rose Bengal stained) and fossil benthic and planktonic foraminiferal species (fractions >63 and >125 μm) from an active pockmark currently releasing methane at Vestnesa Ridge, from gas hydrate mounds from Storfjordrenna (south Svalbard) and from two canyons offshore the Lofoten islands (Northern Norway) characterized by methane-rich sediments. We interpret the results obtained in the context of the sampling environment (i.e, presence/absence of gas hydrates and methane seepage), but also of the foraminiferal ontogeny and ecological preferences (i.e., microhabitat). Finally, we compare the results obtained examining the $\delta^{18}O$ data together with $\delta^{13}C$ data from the same samples. This study represents a significant advancement in the application of the foraminiferal $\delta^{18}O$ in paleoclimatic reconstructions conducted at sites of methane release and gas hydrate dissociation.

2. Study area

This study is based on sediment samples from push cores collected at three geographic locations: 1) Vestnesa Ridge, western Svalbard margin (79°N, 6°E, 1200 m water depth), 2) Storfjordrenna, south Svalbard margin (76°N, 16°E, ~390 m water depth); and 3) an area of the Norwegian margin east of the Lofoten Islands (68°N, 10°W, ~750 m water depth) (Figs. 1 A-D; Table 1). Vestnesa Ridge is a 100 km-long sediment drift oriented SE-NW to E-W

(Talwani and Eldholm, 1977; Thiede et al., 1998; Bünz et al., 2012) characterized by gas hydrate in the subseafloor and methane emitting pockmarks (Bünz et al., 2012; Panieri et al., 2017b). Storfjordrenna is a channel characterized by several mounds (~500 m in diameter and ~10 m in height above the seafloor) constituted by hemipelagic sediments with gas hydrate and carbonate layers of, referred to as gas hydrate mounds (GHM) (Hong et al., 2017, 2018) or gas hydrate pingos (Serov et al., 2017). The third geographic location comprises two canyons situated north of the Trænadjupet slide, on the southern part of the continental Lofoten-Vesterålen slope (Rise et al., 2013). These canyons are ~1.3 km long and 50 m deep relative to surrounding seafloor. Within the canyons, the seafloor is characterized by active methane seepage and microbial mats (Sen et al., 2019); however, there is no evidence for gas hydrates in this area (Rise et al., 2013; Hong et al., 2019).

3. Materials and Methods

3.1 Sediment core collection

Push cores from Vestnesa Ridge were collected in July 2016 using the R/V *G.O. Sars* and the ROV *Ægir 6000*. The sampling was conducted within the two most active pockmarks (Lunde and Lomvi; Figs. 1 A and B). In particular, we collected 7 push cores within the Lunde pockmark (cores V-15, V-16, V-17, V-18, V-19, V-21 and V-25) and 3 push cores within the Lomvi pockmark (cores V-7, V-8 and V-9) (Table 1). The sampling targeted whitish microbial mats (Figs. 1 F and G), indicative of active methane seepage. One push core was collected in the Lunde pockmark in sediments devoid of microbial mats and with no rising methane bubbles (core V-20; Fig. 1E). At this site, head space analysis confirmed the absence of methane. Because of this, we consider this a non-seep reference core.

Multicores from two gas hydrate bearing mounds (GHM) in Storfjordrenna (GHMs 1 and 5) were collected in June 2017 using the R/V Helmer Hanssen and a multicorer equipped with a video camera system (cores 898, 900, 902, 916, 917, 918, 919, 920, 921, and 922; Figs. 1 A and C; Table 1). The push cores from the Lofoten-Vesterålen (LV) canyons were collected in August 2017 during a cruise on board the R/V *G.O. Sars* using the ROV *Ægir 6000* (cores L-8, L-19, L-31, L-32, L-35, L-52, L-56; Figs. 1 A and D; Table 1).

3.2 Pore water analysis

Pore water samples were collected in all cores considered in this study, with the exception of cores V-15 and V-19 (Vestnesa Ridge), where we could not extract enough pore water for sulfate analyses. All pore water samples were measured for sulfate (SO_4^{2-}) except

cores 916, 920, 921, and 922 (Storfjordrenna) because of the low yield. In the LV area, the cores collected in the southern canyon were shared for macro-biology, geochemistry, and micropaleontology investigations. Thus, sulfate profiles were obtained from push cores adjacent to the cores studied for foraminifera. Sulfate concentrations were determined by a Dionex ICS-1100 Ion Chromatograph equipped with a Dionex IonPac AS23 column at the Norwegian Geological Survey (NGU, Trondheim, Norway; Sauer et al., 2016).

Chloride concentrations were measured on pore water samples from cores V-7, V-8, V-9, V-16, V-20, 898, 900, 902, 917, 918, and 919. Chloride concentrations were also determined from the LV canyons cores and reported in Hong et al., (2019). All chloride concentrations were measured onshore also by ion chromatograph (see analytical details in Yao et al. (2019).

The $\delta^{13}C_{DIC}$ was determined on every core analyzed for sulfate, with the exception of cores L-52 and L-56. Measurements were conducted at EAWAG (The Swiss Federal Institute of Aquatic Science and Technology) using an IRMS (Isotope Ratio Mass Spectrometer, Isoprime) equipped with a Gilson 222XL Liquid Handler and a Multiflow unit (Isoprime). Data are reported relative to the Vienna Pee Dee Belemnite (VPDB). The laboratory standard deviation for the VPDB $\delta^{13}C$ was ±0.1‰, based on repeated measurements of the standard. $\delta^{13}C_{DIC}$ from the LV area were measured at Oregan State University (see details for methods in Torres et al., 2005). All pore water raw data are available in supplementary Table a.

3.3 Foraminiferal stable isotope geochemistry

All cores for micropaleontological analysis were sliced on board. Specifically, we collected the first 5 cm of each core at 1-cm resolution at Vestnesa for foraminiferal analyses, with the exception of cores V-15 and V-20 for which only the first 2 cm and first cm, respectively, were available. The same has been done for the first sediment horizon (0-1 cm) in Storfjordrenna and LV samples. All samples were stored in a 2 g L^{-1} Rose Bengal solution in 96 % ethanol, in order to identify living individuals (Walton, 1952). Stained individuals were considered alive or recently alive following Corliss (1991). Prior to washing, samples were stored at 4° C for at least 14 days, following the FOBIMO protocol (Schönfeld et al., 2012), then wet sieved using 63 and 125 µm mesh sieves and dried at 40° C. Foraminifera were picked from the fractions >63 and >125 µm using a stereo microscope.

Isotope measurements ($\delta^{13}C$ and $\delta^{18}O$) were performed on Rose Bengal stained, dead benthic and dead planktonic foraminifera from the 0-1 cm interval of all cores collected at the

three sampled geographic locations (Figs. 1 A-D). In addition, foraminiferal isotope data were collected from the 3-4 cm interval of the Vestnesa Ridge cores. This allowed the comparison of the foraminiferal isotope composition with the most superficial pore water $\delta^{13}C_{DIC}$ data available. On cores V-8 and V-16, the isotopic composition of foraminifera was measured for the entire length of the cores (i.e, 30 and 20 cm for cores V-8 and V-16, respectively).

Foraminiferal $\delta^{13}C$ and $\delta^{18}O$ measurements were conducted at the stable isotope laboratory at UiT – The Arctic University of Norway in Tromsø (Norway) using a Thermo Scientific MAT253 IRMS coupled to a Gasbench II. Species-specific analyses were done on several benthic (*Cassidulina neoteretis*, *Cibicides wuellerstorfi*, *Melonis barleeanus*, *Nonionellina labradorica* and *Trifarina earlandi*) and planktonic (*Neogloboquadrina pachyderma)* foraminiferal species. Recently, it was reported that *M. barleeanus* is characterized by sedimentary particles within its shell, but this mostly influence isotopic data collected using in-situ, rather than bulk, techniques (Borrelli et al., 2018). Foraminiferal shells were placed in 4.5 mL vials and flushed with He gas. Five drops of water-free H_3PO_4 were added manually. After equilibration (>3 hours at 50°C), the samples were analyzed on a Gasbench II and MAT253 Isotope Ratio Mass Spectrometer. Normalization to the VPDB for carbon and oxygen isotopes was done using in-house standards (1.96 ‰, -10.21 ‰, and -48.95 ‰ for $\delta^{13}C$ and -2.15 ‰ and -18.59 ‰ for $\delta^{18}O$). Analytical precision was estimated to be better than 0.07 ‰ for $\delta^{13}C$ and 0.08 ‰ for $\delta^{18}O$ by measuring the certified standard NBS-19. Foraminiferal $\delta^{13}C$ and $\delta^{18}O$ data are reported in supplementary Tables b, c, and d.

Selected specimens were examined by scanning electron microscopy (SEM) and energy dispersive x-ray spectrometry (EDS) to investigate possible diagenetic alterations of the shells. Analyses were performed on several benthic (*Cassidulina neoteretis*, *Melonis barleeanus*, *Nonionellina labradorica and Trifarina earlandi*) and on one planktonic (*Neogloboquadrina pachyderma*) foraminiferal species. 24 specimens have been analyzed and we selected 12 of them to show in this study, based on the quality of the images obtained. The analyzed specimens were chosen from different sediment depths (0-1 cm, 3-4 cm, and 29-30 cm) from cores collected at the three study areas. Specimens were mounted on a circular 25 mm diameter mold using adhesive tape. The mount was then carbon coated and examined with a SEM Hitachi Tabletop Microscope TM-3030 equipped with a Bruker Quantax 70 EDS Detector at UiT. Uncalibrated EDS analyses were performed on the same specimens imaged by SEM to evaluate the elemental composition of the foraminiferal shells and secondary overgrowth.

4. Results

4.1 Pore Water profiles

At Vestnesa Ridge, sulfate concentrations remain fairly constant for core V-20 (our inactive, non-seep control core), and near those of seawater (~28 mM), ranging from 28.4 to 29.6 mM (Fig. 2). Sulfate concentrations in all other cores examined decrease sharply from the seafloor to the bottom of the core. We note that sulfate concentrations in cores V-9 and V-16 are much lower than seawater values, even close to the seafloor (3.6 mM at 2 cm depth and 8.1 mM at 1 cm depth for cores V-9 and V-16, respectively). Except for cores V-18 and V-21, sulfate concentrations are undetectable by 10 cm sediment depth (Fig. 2).

In cores from Storfjordrenna GHM1 (Fig. 3), sulfate profiles at the tops of core have sulfate concentrations similar to that of seawater, with the exception of core 902, where it is 20.2 mM. Sulfate concentrations remain almost constant with depth in cores 898, 917, and 919. A sharp decrease in sulfate concentration with depth is observed in core 902, where sulfate reaches 0.4 mM at 24 cm depth. In cores 900 and 918, sulfate concentration decreases with sediment depth, reaching 2.7 mM at 34 cm and 13.7 mM at 47 cm depth in core 900 and 918, respectively (Fig. 3).

In the LV area, sulfate concentrations were measured on cores from the northern canyon (L-52 and L-56) and from the southern canyon (L-8, L-19, L-31, L-32 and L-35) (Fig. 4). In the southern canyon, cores available for pore water analysis were adjacent to cores studied for foraminifera. Specifically, push core L-9 and push core L-12 were collected next to push cores L-8 and L-19, respectively, whereas push core L-30 was collected next to cores L-31, L-32, and L-35 (Table 1). Overall, the LV canyons cores are characterized by a sharp decrease of sulfate with increasing sediment depth, with the exception of core L-12, which shows constant sulfate concentrations similar to seawater values. In the northern canyon, sulfate reaches very low concentrations around 12 cm depth (cores L-52 and L-56). In the southern canyon, sulfate concentrations are lower than 1 mM below 2 cm in core L-9 and below 6 cm in core L-30 (Fig. 4).

Chloride concentration ranges between 500 and 600 mM and it remains almost constant regardless of sediment depth in all cores analyzed (Figs. 2 and 3). The $\delta^{13}C_{DIC}$ shows values close to 0 in cores V-20 and 898, reflecting the $\delta^{13}C_{DIC}$ signature of normal marine environment (-1 to 1‰; Tagliabue and Bopp, 2008). The $\delta^{13}C_{DIC}$ ranges between -20 and -50 ‰ in the cores collected at Vestnesa Ridge and Storjordrenna GHM1, whereas the cores

collected at the LV canyons are characterized by $\delta^{13}C_{DIC}$ values between -10 ‰ and -70 ‰ (Figs. 2-4).

4.2 Foraminiferal isotopic composition

In this study, we primarly focus on samples collected at Vestnesa Ridge. The presence of gas hydrates at the seafloor and associated gas seepages in the area (Vogt et al., 1994; Hutsoft et al., 2009; Petersen et al., 2010; Bünz et al., 2012; Panieri et al., 2017b), together with the the fact that the cores were collected on microbial mats using a remotely operated vehicle (ROV), make these samples the ideal ones to study the potential effect of gas hydrate dissociation on the foraminiferal $\delta^{18}O$ signature. Hence, at Vestnesa Ridge, we generated complete foraminiferal stable isotope data sets using samples from cores V-8 (30 cm long) and V-16 (20 cm long) (Figs. 1B and 5). We selected these two cores because of the high number of living and dead individuals belonging to *N. pachyderma*, *M. barleeanus*, and *C. neoteretis*. The foraminiferal isotopic composition of *N. pachyderma, C. neoteretis* and *M. barleeanus* was also measured in core V-20, in the interval 0-1 cm (Vestnesa Ridge; Figs. 1B and 5). These values represent the isotopic composition of foraminifera not affected by methane release and oxidation.

The foraminiferal $\delta^{13}C$ values from core V-20 are similar to the foraminiferal $\delta^{13}C$ typical of normal marine conditions (-1 to 1‰; McCorkle et al., 1990), whereas the $\delta^{18}O$ values range from 2.7 to 2.8 ‰ (*N. pachyderma*) and from 4.3 to 4.5 ‰ (*C. neoteretis)*, with *M. barleeanus* recording values from 3.9 to 4 ‰, which are very close to benthic and planktonic values measured in the area (e.g., Consolaro et al., 2017, Schneider et al., 2018).

In samples from cores V-8 and V-16, the *M. barleeanus* $\delta^{13}C$ values range from -2 to -8 ‰, whereas *N. pachyderma* is characterized by values between 1.2 and -14 ‰. In core V-8, we analyzed also *C. neoteretis* and its $\delta^{13}C$ values range from -1.5 to -16 ‰. In general, the foraminiferal $\delta^{13}C$ decreases with increasing sediment depth at core V-8, whereas at core V-16, the $\delta^{13}C$ values decreases from the core surface to a depth of 10 cm and increases afterwards. The trend in foraminiferal $\delta^{18}O$ values is less straightforward. In core V-8, *N. pachyderma* $\delta^{18}O$ ranges from 0.2 to 4.4 ‰, with higher values below 11 cm. On the other hand, the *M. barleeanus* $\delta^{18}O$ ranges from 3.9 to 4.3 ‰, with no trend with increasing sediment depth. The *C. neoteretis* $\delta^{18}O$ varies from 4.6 ‰ to 5.0 ‰ and shows a slight increase with increasing sediment depth. In core V-16, relatively higher $\delta^{18}O$ values were measured in *N. pachyderma* and *M. barleeanus* in samples close to the sulfate methane

transiton (SMT). Below this depth, the $\delta^{18}O$ values decrease only slightly. The *N. pachyderma* $\delta^{18}O$ ranges from 2.3 to 4.2 ‰, whereas the range of *M. barleeanus* $\delta^{18}O$ values is 4.0 to 4.6 ‰.

For cores V-8, V-16, and V-20, isotopic measurements were conducted on planktonic and benthic species from the size fractions >63 μm and >125 μm. Our results do not show a size fraction effect on the $\delta^{18}O$ and $\delta^{13}C$ data. Specifically, a difference of less than 3 % and 6 % difference for $\delta^{18}O$ and $\delta^{13}C$, respectively, is measured between the two size fractions analyzed. The only exception is represented by *M. barleeanus* samples, for which a slight difference between the fractions >63 and >125 μm is observed for the core V-16 $\delta^{13}C$ record.

Additional analyses were conducted on samples from all the other cores collected at Vestnesa Ridge, Storjordrenna, and the LV canyons (Figs. 1 and 6; Table 4). In superficial samples (0-1 cm; Fig. 6A), planktonic foraminiferal $\delta^{18}O$ values are heavier in the GHM Storfjordrenna samples (3-4 ‰) compared to the Vestnesa and LV ones (< 3 ‰). On the contrary, *M. barleeanus* $\delta^{18}O$ values are heavier in cores from Vestnesa Ridge (> 4 ‰ in most of the cores) than in cores from the other sampled areas. The range of $\delta^{18}O$ values is significantly variable in these samples, with planktonic $\delta^{18}O$ values of 1.0 – 4.5 ‰ and benthic $\delta^{18}O$ values of 3.7 – 5.6 ‰. The isotopic signal recorded on living individuals (*C. wuellerstorfi*, *C. neoteretis* and *M. barleeanus*) from Vestnesa Ridge and GHM Storfjordrenna cores does not clearly differ from the values measured in dead foraminifera from the same samples (living-dead difference of 0.6 ‰ for $\delta^{13}C$ and 0.5 ‰ for $\delta^{18}O$).

We note that lower $\delta^{18}O$ values are measured in cores from the LV sites, where heavier benthic (*T. earlandi)* and planktonic (*N. pachyderma*) $\delta^{18}O$ values (2.5 – 3 ‰) coincide to more negative $\delta^{13}C$ values (down to -34.1 ‰). This relationship seems to be present also in the deeper (3-4 cm) samples from Vestnesa Ridge (Fig. 6B), where heavier benthic and planktonic foraminiferal $\delta^{18}O$ (4.5 – 5.5 ‰) coincide to $\delta^{13}C$ values of -11.6 ‰ (*C. neoteretis*) and -15.2 ‰ (*N. pachyderma*). In cores V-8, V-16, and V-20, a similar correspondence between higher $\delta^{18}O$ values and lower $\delta^{13}C$ values is present as well (Fig. 5).

4.3 Foraminiferal microscopy and spectroscopy analyses

Scanning electron microscopy and EDS investigations revealed pristine shells (shells not affected by diagenesis) in superficial samples (0-1 cm) from Vestnesa Ridge and Storfjordrenna (i.e, *C. neoteretis, M. barleeanus, N. labradorica,* and *N. pachyderma;* Figs. 7 A, E, G, and I). Altered shells (shells characterized by carbonate secondary overgrowth) are

identified from the 3-4 cm interval of samples collected at Vestnesa Ridge (*C. neoteretis*, *M. barleeanus*, *N. labradorica*, and *N. pachyderma*; Figs. 7 B, C, D, F, H, and J). Unexpectedly, we found the presence of diagenetic alterations on foraminifera shells in superficial samples (0-1 cm) from cores collected at the LV canyons (*N. pachyderma* and *T. earlandi;* Figs. 7 K and L).

The EDS semi-quantitative analysis show low Mg concentrations in pristine shells (Figs. 7 A, E, and G), even if the EDS map of *N. pachyderma* from core V-8 (0-1 cm; Fig. 7I) reveals a region of high Mg content. Compared to pristine shells, shells affected by diagenesis are characterized by higher Mg concentrations (Figs. 7B, C, D, F, H, and J), with the exception of the superficial samples from the LV canyons where spots of high Ba, rather than Mg, were observed (Figs. 7K and L).

5. Discussion and conclusions

5.1 Geochemical characteristics of gas hydrate and methane-rich sediments

Regions of the seafloor with significant methane are characterized by opposing gradients of pore water sulfate and methane that intersect at a SMT. This is because upward migrating methane can react with sulfate through microbially-mediated anaerobic oxidation of methane (AOM; e.g., Boetius et al., 2000). At the broad scale, the depth of the SMT, though affected by numerous factors, mostly relates to the flux of upward methane (Bhatnagar et al., 2008).

The sharp decrease in sulfate concentration with sediment depth suggests that the SMT is within the first 10 cm in most cores from Vestnesa Ridge except for the inactive, non-seep control core (Fig. 2). The SMT is close to the seafloor in Vestnesa cores V-7, V-8, V-9 and V-16 (less than 10 cm) indicating high methane fluxes putatively advective (Yao et al., 2019). On the contrary, the reference core V-20 displays a sulfate profile typical for marine environments, with no methane influence (Borowski et al., 1996). At Storfjordrenna GHM1, sulfate profiles indicate a deeper SMT (tens of cm), with several cores unable to penetrate the SMT (Fig. 3). In the LV canyons (Fig. 4), the SMT seems close to the seafloor (~5 cm) in the southern canyon, with the exception of core L-12, deeper (10-15 cm) in the northern canyon (core L-52).

The AOM reaction produces hydrogen sulfide and bicarbonate, the latter which comprises most of DIC in marine settings. Universally, the DIC in sediment pore waters is depleted in ^{13}C around SMT (e.g., Torres et al., 2003; Ussler et al., 2008), due to both the ^{13}C-depleted methane as the carbon source and isotopic fractionation associated with this

microbial process (Borowski et al., 1997; Hong et al., 2013; Yoshinaga et al., 2014). The actual $\delta^{13}C$ value of DIC at the SMT is complicated. Methane can derive from thermogenic ($\delta^{13}C$: -55 ‰ to -40 ‰) or microbial ($\delta^{13}C$: -100 ‰ to -55 ‰) sources (Whiticar, 1999); DIC enriched in ^{13}C and formed during methanogenesis can also migrate upward (Chatterjee et al., 2011).

The $\delta^{13}C_{DIC}$ profiles (Figs. 2-4) reveal depleted values at cores V-7, V-8, V-9, V-16, V-17, V-18, and V-21 from Vestensa Ridge; cores 900, 902, 917, 918, and 919 from Storfjordrenna, and cores L-9, L-12, and L-30 from the LV canyons. Core V-20 is the only core at Vestnesa Ridge that records the $\delta^{13}C_{DIC}$ values similar to modern normal marine environment (-1 to 1‰; Tagliabue and Bopp, 2008), confirming that this core is not affected by methane seepage and oxidation. Core 898 also shows $\delta^{13}C_{DIC}$ values similar to the modern normal marine environment. In all other cores investigated, the negative $\delta^{13}C_{DIC}$ values suggest that cored sites are influenced by upward methane fluxes (e.g., Whiticar et al., 1999). In GHM cores, we cannot exclude a signal reflecting organiclastic sulfate reduction, which occurs between the seafloor and the SMT and is characterized by depleted but greater $\delta^{13}C_{DIC}$ than AOM (Chatterjee et al., 2011).

The chloride profiles available from Vestnesa Ridge and Sorfhordrenna GHM1 (Figs. 2 and 3) do not vary with sediment depth, suggesting that the sampling sites are not affected by fluid migration of a low-chloride fluid through the sediment column.

5.2 Foraminiferal evidences of gas hydrate emission

5.2.1 Foraminiferal stable isotope compositions

Overall, the isotopic compositions of Rose Bengal stained (‘living’) foraminifera do not substantially differ from other values reported in literature. In fact, specimens of *C. neotretis* and *N. pachyderma* from the top of the control core V-20 (0-1 cm; Fig. 5), which has no evidence for upward methane migration, exhibit values consistent with other studies in the region (e.g., Consolaro et al., 2015; Schneider et al., 2018). There is also a clear distinction between planktonic and benthic $\delta^{13}C$ and $\delta^{18}O$ values. Vital effects and ecological preferences (e.g., microhabitat), but also environmental parameters (e.g., temperature, pH), all influence the isotopic composition of the foraminiferal shells (Duplessy et al., 1970; Bemis et al., 1998; Ravelo and Hillaire Marcel, 1999; Barras et al., 2010). In this context, we interpret the offset between the $\delta^{18}O$ of *C. neotretis* and *N. pachyderma* as a consequence of different habitats for these species (e.g., Kennett et al., 2000; Consolaro et al., 2015). Ecological preferences

(Murray, 2006) might also explain the small differences in stable isotope compositions between *C. neoteretis* (a shallow infaunal species) and *M. barleeanus* (an intermediate infaunal species). Notably, the former has higher $\delta^{13}C$ and $\delta^{18}O$.

However, of all foramifera samples examined, the most depleted $\delta^{13}C$ value (-5.7 ‰) was measured in Rose Bengal stained *N. labradorica*, a deep infaunal species (Racine et al., 2018). We note that the depleted $\delta^{13}C$ value we measured in this species is similar to the $\delta^{13}C$ signature measured in another living deep infaunal foraminifer from Monterey Bay (*Globobulimina pacifica;* -6 ‰; Bernhard et al., 2010). We believe that these $\delta^{13}C$ values represent a 'threshold' of the isotopic composition of non-diagenetically altered foraminifera inhabiting seep sites. It might be possible that the depleted $\delta^{13}C$ measured in our living *N. labradorica* is a consequence of vital effects. However, considering the sampling location, we think that the *N. labradorica* $\delta^{13}C$ is the result of the incorporation of methane derived ^{13}C-depleted carbon during shell formation and likely ingestion of ^{13}C-depleted methanotrophic microbes (Rathburn et al., 2003; Panieri, 2006; Bernhard and Panieri, 2018).

In gas hydrate bearing sediments, the $\delta^{18}O$ of pore water can be affected by gas hydrate formation and dissociation because the water trapped in gas hydrates is more enriched in ^{18}O compared to the adjacent pore water (Davidson et al., 1983; Tomaru et al., 2006; Ijiri et al., 2018). With the data available, we cannot draw a firm conclusion regarding the possibility that the $\delta^{18}O$ signature of living benthic foraminifera can record episodes of gas hydrate dissociation. Our data indicate that living foraminifera cannot record gas hydrate dissociation as shell formation is a discontinuous and brief process that might not be coeval with episodes of gas hydrate decomposition, which are also transient in time (Thatcher et al., 2013; Anderson et al., 2014). It might be equally possible that the $\delta^{18}O$ signature of living benthic foraminifera does not reflect the influence of gas hydrate dissociation, because no dissociation happened during the life span of the specimens analyzed. However, a different interpretation can be drawn when considering foraminifera with diagenetic overgrowth.

Over relatively long time scales (Plio-Peistocene), gas hydrate dissociation can alter the carbonate system and the MDAC isotopic signature (Bohrmann et al., 1998; Crémière et al., 2016), as revelaed by a recent study showing a disequilibrium between carbonate crust clumped isotopes and the expected temperature of formation (Loyd et al., 2016). In cores V-8 and V-16, the slight downcore increase in the *C. neoteretis* and *M. barleeanus* $\delta^{18}O$ (up to 5 ‰) values compared to the reference-like values of core V-20 suggest the possible influence of gas hydrate dissociation on the $\delta^{18}O$ signature of fossil foraminifera through sedimentary

overgrowth. The variability in the *N. pachyderma* $\delta^{18}O$ values (1.8 to 4.5 ‰) from cores V-8 and V-16 supports this hypothesis.

It was proposed that the planktonic foraminiferal isotopic composition can be influenced by hydrate dissociation (Maslin et al., 2005). However, in this work, the precipitation of authigenic carbonate around the foraminiferal shells was not discussed. Cores V-8 and V-16 are located at ~1,200 m water depth. Thus, methane seepage at these locations is rapidly dispersed in the ocean or microbially oxidized to CO_2 in the water column (Damn et al., 2005; Steinle et al., 2015), making it improbable that living planktonic foraminifera can record episodes of gas hydrate dissociation and methane oxidation (e.g., Consolaro et al., 2018). However, evidence of gas hydrate dissociation can be recorded after the death and burial of planktonic species, in particular at the depth of the SMT, where MDAC can precipitate on the foraminiferal shells (Panieri et al., 2016; Schneider et al., 2018).

In this study, the wide range of $\delta^{18}O$ values measured in both planktonic and benthic foraminiferal shells confirms that the isotopic composition of *N. pachyderma* and *C. neoteretis* is a consequence of the precipitation of ^{18}O-rich authigenic carbonates (see also next section). Our conclusion is in agreement with other studies conducted at different geographic locations (Fig. 6). For example, Torres et al. (2003) estimated that the range of $\delta^{18}O$ values (0-1.75 ‰) measured on foraminiferal calcite from the Hydrate Ridge was due to 22 wt.% (authigenic) carbonates precipitated around the shells. Heavier foraminiferal $\delta^{18}O$ (range from 2 to 4 ‰) were reported also for dead foraminifera from methane vents environments in the Gulf of California (Herguera et al., 2014). Also in this case, the foraminiferal isotopic composition was interpreted to be influenced by authigenic carbonates. Those results are in agreement with the range of data measured in our study areas (Fig. 6A). At Vestnesa Ridge, the identification of authigenic carbonate precipitated on foraminiferal tests from deeper sediments (several meters of sediment depth) points out the same depleted $\delta^{13}C$ and heavy $\delta^{18}O$ (Schneider et al., 2017; Fig. 6B).

Secondary overgrowth affected planktonic and benthic foraminifera alike, even if the ^{18}O enrichment is more evident in *N. pachyderma* because of the lower $\delta^{18}O$ values recorded by this species in marine environments not affected by methane (e.g. core V-20). In addition, similar $\delta^{18}O$ enrichments to the ones we measured in foraminifera were reported for MDAC from gas hydrate and cold seeps settings (Greinert et al., 2001, 2010; Eichhubl and Boles, 1998; Eichhubl et al., 2000; Naehr et al., 2007, 2009; Crémière et al., 2016).

Gas hydrate dissociation, and consequent release of ^{18}O-enriched water is a process that takes place below the SMT, wile ^{13}C-depleted methane is present within the SMT. This would suggest that gas hydrate dissociation might not be associated with foraminiferal low $\delta^{13}C$ and high $\delta^{18}O$ values. However, our results clearly show a relationship between depleted $\delta^{13}C$ and enriched $\delta^{18}O$ values in foraminifera, in particular in cores V-8 and V-16, collected at gas hydrate bearing sediments where the SMT is close to the seafloor (Fig. 5).

We recognize that the foraminiferal $\delta^{18}O$ can vary because of changes in environmental parameters that are unrelated to gas hydrate dissociation. However, we do not think that this is the case for the samples analyzed in this study for several reasons. First, we observe a wide range of $\delta^{18}O$ values on both planktonic and benthic foraminifera even within the first few centimenters of sediment (Figs. 5 and 6). At Vestnesa Ridge, this difference in $\delta^{18}O$ values would translate in several degrees C difference in less than a millennium, if we take into account the modern sedimentation rate at this location (~19 cm/kyrs; Consolaro et al., 2015). We think that such a big temperature change in a short time frame is highly unlikely. In fact, this change would be more abrupt than temperature shifts characterizing the Heinrich events over the Pliocene (Cortijo et al., 1997). We note that a similar variability in the foraminiferal $\delta^{18}O$ as recorded in the Vestnesa Ridge samples was measured in surface sediments from the LV canyons (0-1 cm; Fig. 6A), confirming that a temperature change cannot be a likely explanation of our data, within the same 1 cm-sediment layer.

Second, similar foraminiferal $\delta^{18}O$ ranges from cold seep sites as the ones recorded in surface samples at Vestnesa Ridge (Fig. 6A) have not often been reported in literature, with a few exceptions possible as a consequence of temperature changes among the sites analyzed (e.g., 2 ‰ in Sen Gupta and Aharon, 1994; 1.35 ‰ in Burkett et al., 2018). Burkett et al. (2018) observed a maximum $\delta^{18}O$ increase of +0.7 ‰ in cold seeps that they interpreted to be the consequence of fluids impact. Considering our stable Chloride profiles together with the heat flow estimated in the Vestnesa Ridge, leading to heat excess of less than 0.04°C at 50 cm sediment depth (Bohrmann et al., 2016), we exclude this hypothesis.

Third, clay dehydration through the smectite transformation into illite can cause a ^{18}O enrichment of pore waters. This diagenetic process occurs in deep sediments at temperature ranging from 60° to 160° C (~1000 m below sea floor). However, the Chloride profiles at Vestnesa Ridge and Storfjordrenna GHM do not support any clay dehydration, as observed also in mud volcano systems (Hensen et al., 2004). Yet, we cannot exclude an impact of meteoric fluids in the LV canyons, as documented by Hong et al. (2019), with a different $\delta^{18}O$

signature, even though the correlation between depleted $\delta^{13}C$ and heavy $\delta^{18}O$ points to the presence of authigenic carbonate on foraminiferal shells. Consequently, we do not think that clay dehydration, temperature, or salinity changes can affect the pore water of surface sediments in our three study areas.

Finally, the size fraction analyzed might also cause biases in the isotopic records used to interpret short time-scale processes because the isotopic composition of large foraminifera (>150 μm) can reflect a longer-term averaged calcification process that is not influenced by episodic processes (i.e, eutrophic periods or seasonal changes; Fontanier et al., 2006). In addition, ontogenic effects are reported in literature for both planktonic (e.g., Spero et al., 1997; Elderfield et al., 2002) and benthic (e.g., Friedrich et al., 2006; Barras et al., 2010; Schumacher et al., 2010) foraminifera. The analysis of different size fractions (150, 250, 350, 450, 550, 650 and 750 μm) by Corliss et al. (2002) did not reveal a seasonal influence on the foraminiferal isotopic record, suggesting the absence of an ontogenetic effect on the foraminiferal isotope incorporation. The foraminiferal isotope data we collected using different size fractions (i.e., >63 and >125 μm) are in agreement with the conclusions reached by Corliss et al. (2002), demonstrating that the benthic and planktonic foraminiferal $\delta^{18}O$ values are very similar in both fracions analyzed and that they are not biased by ontogenetic effects.

5.2.2 Foraminiferal secondary overgrowth

Our SEM analyses revealed significant visual diagenetic alteration on several of the foraminiferal shells analyzed, but not on all of them. Living individuals of *N. labradorica* and *M. barleeanus* from Storfjordrenna GHM1 (Figs. 7 E and G) were not affected by diagenetic alteration, even if we measured relatively low $\delta^{13}C$ in these samples. This suggest that the depleted $\delta^{13}C$ signature of these samples was incorportated in the primary foraminiferal calcite (calcite deposited by the foraminifera during shell growth), as proposed in other studies (e.g., Panieri et al., 2017a, Schneider et al., 2017; Wan et al., 2018).

Diagenetic features were confirmed by EDS maps of samples collected deeper in the sediment column. In particular, we interpret the high Mg concentration to be the evidence of the presence of secondary overgrowth on the shells analyzed (e.g., Panieri et al., 2017a; Schneider et al., 2017). In the 3-4 cm sediment horizon, diagenetic alterations were observed in different Vestnesa pockmarks (*C. neoteretis* from cores V-8 and V-16; Fig. 7 B and C), suggesting that precipitation of MDAC on foraminiferal shells occurs at a regional scale. The

C. neoteretis collected at deeper sediment depths (core V-8, 29-30 cm; Fig. 7D) is characterized by the highest Mg content.

The samples from the LV canyon south did not reveal high concentrations of Mg, but an enrichment in Ba (Fig. 7 K and L). Ba-calcite has been described as a product of early diagenesis (Dejonghe and Boulvain, 1993; Schroeder et al., 1997), which can affect foraminiferal carbonate (Lea and Boyle, 1993). Barite in seafloor crusts as well as high dissolved Ba concentration have been described in the LV area (Sen et al., 2019; Hong et al., 2019) and EDS analysis of foraminiferal shells show an initial possible precipitation of authigenic Ba-rich overgrowth. Further investigations are needed to understand if these overgrowths can impact the foraminiferal isotopic composition in samples from the LV canyons and other geographic locations. Overall, our microscopy and spectroscopy analyses confirm the hypothesis that the isotopic composition measured in fossil foraminifera is affected by secondary overgrowth precipitated on the foraminiferal shells at the SMT and that this signal is related to methane oxidation and gas hydrate dissociation.

Nevertheless, isotopic composition of fossil foraminifera might also depend on the secondary overgrowth mineralogy. In fact, the mineralogy of MDAC usually include microcrystalline Mg-calcite, aragonite, and dolomite (e.g., Roberts and Aharon, 1994, Bohrmann et al., 1998, Crémière et al., 2012; Sauer et al., 2017). Different types of carbonate have different oxygen isotopic fractionation (e.g., Kim et al., 2007; Vasconcelos et al., 2005). For example, dolomite is estimated to show an enrichment of 5 to 7 ‰ of ^{18}O compared to synthetic calcite (O'Neil and Epstein, 1966). At methane cold seeps, a wide range of $\delta^{18}O$ has been related to the mineralogy of authigenic carbonates (e.g., Orphan et al., 2004; Gieskes et al., 2005), with $\delta^{18}O$ values up to 7.5 ‰ in high Mg-calcite, while aragonite displayed lighter $\delta^{18}O$.

The ^{18}O enrichment in authigenic carbonate rocks has been interpreted as evidence for gas hydrate dissociation at several methane seep and non-seep environments (e.g., Bohrmann et al., 1998: Aloisi et al., 2000; Pierre et al., 2002; Conti et al., 2004). At these sites, the heavy $\delta^{18}O$ of Mg-calcite was used as an evidence for gas hydrate dissociation, whereas the origin of light aragonite $\delta^{18}O$ remains uncertain. It is possible that this difference is a consequence of Mg-calcite and aragonite precipitating from two highly distinct pore-water conditions (Bohrmann et al., 1998), even if the chemical controls on the carbonate phase that precipitates are still not completely understood (Burton, 1993). Schneider et al. (2017) estimated that the authigenic carbonate proportion on foraminiferal tests can be up to 58 %. A calcite containing

50 % of Mg-$CaCO_3$ is expected to be enriched in ^{18}O by 3-4 ‰ (Tarutani et al., 1969; Fritz and Smith, 1970).

Finally, in this study, we demonstrate that at methane seeps and gas hydrate bearing sediments fossil planktonic and benthic foraminifera are characterized by relatively high $\delta^{18}O$ values. We propose that this ^{18}O enrichment is related to past gas hydrate dissociation event(s). Hydrate dissociation release ^{18}O-enriched water, which affect the pore water isotopic signature. This signal can be incorporated by authigenic carbonates precipitating around foraminiferal shells at the SMT. In addition, we speculate that mineralogy of the secondary overgrowth might also influence the isotopic signal measured in fossil foraminifera.

Acknowledgments

The authors wish to thank the captain and the crew of the R/V G.O. Sars and Helmer Hanssen. This study has been funded by the project Petromaks2 Norcrust – Norwegian margin fluid systems and methane-derived authigenic carbonate crusts (project no. 255150) and the Research Council of Norway through CAGE Center for Excellence in Arctic Gas Hydrate Environment grant 287 no. 223259.

References

Aloisi, G., Pierre, C., Rouchy, J.-M., Foucher, J.-P., Woodside, J., the MEDINAUT Scientific Party, 2000. Methane-related authigenic carbonates of eastern Mediterranean Sea mud volcanoes and their possible relation to gas hydrate destabilization. Earth and Planetary Science Letters 184, 321-338. https://doi.org/10.1016/S0012-821X(00)00322-8.

Anderson, B., Boswell, R., Collett, T.S., Farrell, H., Ohtsuki, S., White, M., Zyrianova, M., 2014. Review of the findings of the Ignik Sikumi CO_2-CH_4 gas hydrate exchange field trial. In: Proceedings of the international conference on gas hydrates, Beijing; 2014.

Barras, C., Duplessy, J.-C., Geslin. E., Michel, E., Jorissen, F.J., 2010. Calibration of $\delta^{18}O$ of cultured benthic foraminiferal calcite as a function of temperature. Biogeosciences 7, 1349-1356.

Barbieri, R. and Panieri, G., 2004. How are benthic foraminiferal faunas influenced by cold seeps? Evidence from the Miocene of Italy. Palaeogeography, Palaeoclimatology, Palaeoecology 204, 257-275.

Bemis, B.E., Spero, H.J., Bijma, J., Lea D.W., 1998. Reevaluation of the oxygen isotopic composition of planktonic foraminifera: experimental results and revised paleotemperature equations. Paleoceanography 13 (2), 150 – 160.

Bernhard, J.M. and Panieri, G., 2018. Keystone Arctic paleoceanographic proxy association with putative methanotrophic bacteria. Scientific Reports 8, 10610.

Bernhard, J.M., Martin, J.B., Rathburn, A., 2010. Combined carbonate carbon isotopic and cellular ultrastructural studies of individual benthic foraminifera: 2. Toward an understanding of apparent disequilibrium in hydrocarbon seeps. Paleoceanography 25, PA4206, doi:10.1029/2010PA001930

Bhatnagar, G., Chapman, W.G., Dickens, G.R., Dugan, B., Hirasaki, G.J., 2008. Sulfate-methane transition as a proxy for average methane hydrate saturation in marine sediments. Geophysical Research Letters 35, L03611. doi:10.1029/2007GL032500.

Boetius, A., Ravenschlag, K., Schubert, C. J., Rickert, D., Widdel, F., Gieseke, A., Amann, R., Jorgensen, B. B., Witte, U., and Pfannkuche, O., 2000. A marine microbial consortium apparently mediating anaerobic oxidation of methane, Nature, 407, 623-626.

Bohrmann, G., Greinert, J., Suess, E., Torres, M., 1998. Authigenic carbonates from the Cascadia subduction zone and their relation to gas hydrate stability. Geology 26, 647-650. https://doi.org/10.1130/0091-7613(1998)026<0647:ACFTCS>2.3.CO;2.

Bohrmann, G., Ahrlich, F., Bergenthal, M., Bünz, S., Düßmann, R,. Ferreira, Ch., Freudenthal, T., Fröhlich, S., Hamann, K., Hong, W.-L., Hsu, Ch.-W., Johnson, J., Kaszemeik, K., Kausche,A., Klein, T., Lange, M., Lepland, A., Malnati, J., Meckel, S., Meyer-Schack, B., Noorlander, K., Panieri, G., Pape, T., Reuter, M., Riedel, M., Rosiak, U., Schmidt, Ch., Schmidt, W., Seiter, Ch., Spagnoli, G., Stachowski, A., Stange, N., Wallmann, K., Wintersteller, P., Wunsch, D., Yao, 2016. H.R/V MARIA S. Merian Cruise Report MSM57: http://nbn-resolving.de/urn:nbn:de:gbv:46-00105895-15

Borowski, W.S., Paull, C.K., Ussler, W., 1996. Marine pore-water sulfate profiles indicate in situ methane flux from underlying gas hydrate. Geology 24, 655-658.

Borowski, W. S., Paull, C. K., and Ussler, W., 1997. Carbon cycling within the upper methanogenic zone of continental rise sediments: An example from the methane-rich sediments overlying the Blake Ridge gas hydrate deposits, Marine Chemistry, 57, 299-311.

Borrelli, C., Panieri, G., Dahl, T.M., Neufeld, K., 2018. Novel biomineralization strategy in calcareous foraminifera. Scientific Reports 8, 10201.

Bünz, S., Polyanov, S., Vadakkepuliyambatta, S., Consolaro, C., Mienert, J., 2012. Active gas venting through hydrate-bearing sediments on the Vestnesa Ridge, offshore W Svalbard. Marine Geology 332–334, 189–197. http://dx.doi.org/10.1016/j.margeo.2012.09.012.

Burkett, A.M., Rathburn, A., Elena Pérez, M., Martin, J.B., 2018. Influences of thermal and fluid characteristics of methane and hydrothermal seeps on the stable oxygen isotopes of living benthic foraminifera. Marine and Petroleum Geology 93, 344-355.

Burton, E.A., 1993. Controls on marine carbonate cement mineralogy: Review and reassessment. Chemical Geology 105, 163–179.

Chatterjee, S., Dickens, G. R., Bhatnagar, G. Chapman, W. G., Dugan, B., Snyder, G. T., Hirasaki, G.J., 2011. Pore water sulfate, alkalinity, and carbon isotope profilesin shallow sediment above marine gas hydrate systems:A numerical modeling perspective. Journal of Geophysical Research 116, B09103. doi:10.1029/2011JB008290.

Consolaro, C., Rasmussen, T.L., Panieri, G., Mienert, J., Bünz, S., Sztybor, K., 2015. Carbon isotope ($\delta^{13}C$) excursions suggest times of major methane release during the last 14 kyr in Fram Strait, the deepwater gateway to the Arctic. Climate of the Past 11, 669–685. http://dx.doi.org/10.5194/cp-11-669-2015.

Consolaro, C., Rasmussen, T.L., Panieri, G., 2018. Palaeoceanographic and environmental changes in the eastern Fram Strait during the last 14,000 years based on benthic and planktonic foraminifera. Marine Micropaleontology 139, 84-101. https://doi.org/10.1016/j.marmicro.2017.11.001

Conti, S., Fontana, D., Gubertini, A., Sighinolfi, G., Tateo, F., Fioroni, C., Fregni, P., 2004. A multidisciplinary study of middle Miocene seep-carbonates from the northern Apennine foredeep (Italy). Sedimentary Geology 169, 1-19.

Corell, R.W., Hassol, S.J., Melillo, J., 2008: Emerging Challenges – Methane from the Arctic: Global warming wildcard, UNEP Year Book 2008: An Overview of Our Changing Environment, United Nations Environment Programme, Stevenage, Hertfordshire, UK.

Corliss, B.H. (1991), Morphology and microhabitat preference of benthic foraminifera from the northwest Atlantic Ocean, Mar. Micropaleontology, 17(3-4), 195-236, doi:10.1016/0377-8398(91)90014-W.

Corliss, B.H., McCorkle, B.C., Higdon, D.M., 2002. A time series study of the carbon isotopic composition of deep-sea benthic foraminifera. Paleoceanography 17, 1-27. https://doi.org/10.1029/2001PA000664.

Cortijo, E., Labeyrie, L., Vidal, L., Vautravers, M., Chapman, M., Duplessy, J.-C., Elliot, M., Arnold, M., Turon, J.-L., Auffret, G., 1997. Changes in sea surface hydrology associated with Heinrich event 4 in the North Atlantic Ocean between 40° and 60°N. Earth and Planetary Science Letters 146, 29-45.

Crémière, A., Pierre, C., Blanc-Valleron, M.-M., Zitter, T., Namik Çağatay, M., Henry, P., 2012. Methane-derived authigenic carbonates along the North Anatolian fault system in the Sea of Marmara (Turkey). Deep Sea Research Part I: Oceanographic Research Papers 66, 114-130.

Cremiere, A., Lepland, A., Chang, S., Sahy, D., Condon, D. J., Noble, S. R., Martma, T., Thorsnes, T., Sauer, S., and Brunstad, H., 2016. Timescales of methane seepage on the Norwegian margin following collapse of the Scandinavian ice sheet, Nature communications.

Damm, E., Mackensen, A., Budeus, G., Faber, E., Hanfland, C., 2005. Pathways of methane in seawater: Plume spreading in an Arctic shelf environment (SW-Spitsbergen). Continental Shelf Research 25, 1453-1472.

Davidson, D. W., Leaist, D.G., Hesse, R., 1983. Oxygen-18 enrichment in the water of a clathrate hydrate. Geochimica et Cosmochimica Acta 47, 2293-2295.

Dickens, G.R., J.R. O'Neil, D.K. Rea, and R.M. Owen (1995), Dissociation of oceanic methane hydrate as a cause of the carbon isotope excursion at the end of the Paleogene, Paleoceanography, 10(6), 965-971, doi:10.1029/95PA02087.

Duplessy, J.-C., Lalou, C., Claude Vinnot, A., 1970. Differential Isotopic Fractionation in Benthic Foraminifera and Paleotemperatures Reassessed. Science 10, 250-251.

Eichhubl, P., Boles, J.R., 1998. Vein formation in relation to burial diagenesis in the Miocene Monterey Formation, Arroyo Burro Beach, Santa Barbara, California. In: Eichhubl. P. (Ed.), Diagenesis, Deformation, and Fluid Flow in the Miocene Monterey Formation of coastal California. SEPM Pacific Section Special Publication 83, pp. 15–36.

Eichhubl, P., Greene, H. G., Naehr, T., Maher, M., 2000. Structural control of fluid flow: offshore fluid seepage in the Santa Barbara Basin, California. Journal of Geophysical Exploration 69-70, 545-549. https://doi.org/10.1016/S0375-6742(00)00107-2.

Elderfield, H., Vautravers, M., Cooper, M., 2002. The relationship between shell size and Mg/Ca, Sr/Ca, δ18O, and δ13C of species of planktonic foraminifera. Geochenistry, Geophiscs, Geosystems 3, 1-13.

Dejonghe, L., Boulvain, F., 1993. Paleogeographic and diagenetic context of a baritic mineralization enclosed within Frasnian peri-reefal formations: Case history of the Chaudfontaine mineralization (Belgium). Ore Geology Reviws 7, 413-431.

Duplessy, J.-C., Lalou, C., Vinot, A.C., 1970. Differential isotopic fractionation in benthic foraminifera and paleotemperatures reassessed. Science 168, 250 – 251.

Fontanier, C., Mackensen, A., Jorissen, F.J., Anschutz, P., Licari, L., Griveaud, C., 2006. Stable oxygen and carbon isotopes of live benthic foraminifera from the Bay of Biscay: Microhabitat impact and seasonal variability. Marine Micropaleontology 158, 159-183. https://doi.org/10.1016/j.marmicro.2005.09.004.

Friedrich, O., Schmiedl, G., Erlenkeuser, H., 2006. Stable isotope composition of Late Cretaceous benthic foraminifera from the southern South Atlantic: Biological and environmental effects. Marine Micropaleontology 58, 135-157.

Fritz and Smith, 1970. The isotopic composition of secondary dolomites, Geochimlca et Cosmochimica Acta. 34, pp. 1101-1173.

Greinert, J., Bohrmann, G., Suess, E., 2001. Gas Hydrate-Associated Carbonates and Methane-Venting at Hydrate Ridge: Classification, Distribution, and Origin of Authigenic

Lithologies. In: Paull CK, Dillon WP (eds) Natural gas hydrates: occurrence, distribution, and detection. Geophysical Monograph series 124, 99–113.

Greinert, J., Bialas, J., Lewis, K., Suess, E., 2010. Methane seeps at the Hikurangi Margin, New Zealand. Marine Geology 272, 1-3.

Gieskes, J., Mahn, C., Day, S., Martin, J. B., Greinert, J., Rathburn, T., McAdoo, B., 2005. A study of the chemistry of pore fluids and authigenic carbonates in methane seep environments: Kodiak Trench, Hydrate Ridge, Monterey Bay, and Eel River Basin. Chemical Geology 220, 329-345. https://doi.org/10.1016/j.chemgeo.2005.04.002.

Hensen, C., Wallmann, K., Schmidt, M., Ranero, C.R., Suess, E., 2014. Fluid expulsion related to mud extrusion off Costa Rica—A window to the subducting slab. Geology 32, 201-204.

Herguera, J.C., Paull, C.K., Perez, E., Ussler, W., Peltzer, E., 2014. Limits to the sensitivity of living benthic foraminifera to pore water carbon isotope anomalies in methane vent environments. Paleoceanography 29, 273-289.

Hill, T.M., Kennett, J.P., Spero, H.J., 2003. Foraminifera as indicators of methane-rich environments: A study of modern methane seeps in Santa Barbara Channel, California. Marine Micropaleontology 49, 23-138.

Hong, W.-L., Torres, M. E., Kim, J.-H., Choi, J., and Bahk, J.-J., 2013. Carbon cycling within the sulfate-methane-transition-zone in marine sediments from the Ulleung Basin, Biogeochemistry, 1-20, 10.1007/s10533-012-9824-y.

Hong, W.-L., Torres, M.E., Carroll, J., Cremiere, A., Panieri, G., Yao, H., Serov, P., 2017. Seepage from an Arctic shallow marine gas hydrate reservoir is insensitive to momentary ocean warming. Nature Communications. https://doi.org/10.1038/ncomms15745.

Hong, W.-L., Torres, M.E., Portnov, A., Waage, M., Haley, B., Lepland, A., 2018. Variations in Gas and Water Pulses at an Arctic Seep: Fluid Sources and Methane Transport. Geophysical Research Letters 45 https://doi.org/10.1029/2018GL077309.

Hong, W.-L., Lepland, A., Himmler, T., Kim, J.-H., Chand, S., Sahy, D., D., Solomon, E., Rae, J., Tonu, M., Nam, S.-I., and Knies, J., 2019. Discharge of meteoric water in the eastern

Norwegian Sea since the last glacial period. Geophysical Research Letters, 46. https://doi.org/10.1029/2019GL084237.

Hustoft, S., Bünz, S., Mienert, J., Chand, S., 2009. Gas hydrate reservoir and active methane-venting province in sediments on < 20 Ma young oceanic crust in the Fram Strait, offshore NW-Svalbard. Earth and Planetary Science Letters 284, 12-24. http://dx.doi.org/10.1016/j.epsl.2009.03.038.

Ijiri, A., Inagaki, F., Kubo, Y., Adhikari, R.R., SHattori, S., Hoshino, T., Imachi, H., Kawagucci, S., Morono, Y., Ohtomo, Y., Ono, S., Sakai, S., Takai, K., Toki, T., Wang, D.T., Yoshinaga, M.Y., Arnold, G.L., Ashi, J., Case, D.H., Feseker, T., Hinrichs, K.-U., Ikegawa, Y., Ikehara, M., Kallmeyer, J., Kumagai, H., Lever, M.A., Morita, Nakamura, K.-I., Nakamura, Y., Nishizawa, M., Orphan, V.J., Røy, H., Schmidt, F., Tani, A., Tanikawa, W., Terada, T., Tomaru, H., Tsuji, T., Tsunogai, U., Yamaguchi Y.T., Yoshida, N., 2018. Deep-biosphere methane production stimulated by geofluids in the Nankai accretionary complex. Science Advances, 4(6), 1– 15. https:/doi.org/10.1126/sciadv.aao4631

IPCC, 2013. Climate Change 2013: The Physical Science Basis. Contribution of Working Group I to the Fifth Assessment Report of the Intergovernmental Panel on Climate Change. In T.F. Stocker and others [eds.], Cambridge Univ. Press.

Jakobsson, M., Spielhagen, R.F., Thiede, J., Andreasen, C., Hall, B., Ingólfsson, Ó., Kjær, K. H., Van Kolfschoten, T. , Krinner, G., Long, A., Lunkka, J.-P., Subetto, D., Svendsen, J.I., 2008. Foreword to the special issue: Arctic paleoclimate and its extremes (APEX), Polar Res., 27(2), 97-104, doi:10.1111/j.1751-8369.2008.00063.x.

James, R.H., Bousquet, P., Bussmann, I., Haeckel, M., Kipfer, R., Leifer, I., Niemann, H., Ostrovsky, I., Pizkozub, J., Rehder, G., Treude, T., Vielsdädte, L., Greinert, J., 2016. Effects of climate change on methane emissions from seafloor sediments in the Arctic Ocean: A review. Limnology and Oceanography 61, 283–299. doi: 10.1002/lno.10307

Kennett, J.P., Cannariato, K.G., Hendy, I.L., Behl, R.J., 2000. Carbon isotopic evidence for methane hydrate instability during quaternary interstadials. Science 288, 128–133.

Kim, S.-T., O'Neil, J.R., Hillaire-Marcel, C. and Mucci, A., 2007. Oxygen isotope fractionation between synthetic aragonite and water: Influence of temperature and Mg2+ concentration. Geochimica et Cosmochimica Acta 71, 4704-4715.

Kvenvolden, K.A. 1988. Methane hydrate—a major reservoir of carbon in the shallow geosphere. Chemical Geology 71: 41–51. doi:10.1016/0009-2541(88)90104-0

Lea, D.W., Boyle, E.A., 1993. Determination of carbonate-bound barium in foraminifera and corals by isotope dilution plasma-mass spectrometry. Chemical Geology 103, 73-84.

Loyd S.J., Sample, J., Tripati, R.E., Defliese, W.F., Brooks, K., Hovland, M., Torres, M., Marlow, J., Hancock, L.G., Martin, R., Lyons, T., Tripati, A.E., 2016. Methane seep carbonates yield clumped isotope signatures out of equilibrium with formation temperatures. Nature Communications 7:12274. DOI: 10.1038/ncomms12274.

Martin, R.A., Nesbitt, E.A., Campbell, K.A., 2007. Carbon stable isotopic composition of benthic foraminifera from Pliocene cold methane seeps, Cascadia accretionary margin. Paleogeography, Paleoclimatolgy, Paleoecology 246, 260-277.

Martin, R.A., Nesbitt, E.A., Campbell, K.A., 2010. The effects of anaerobic methane oxidation on benthic foraminiferal assemblages and stable isotopes on the Hikurangi Margin of eastern New Zealand. Marine Geology 272, 270–284. doi:10.1016/j.margeo.2009.03.024.

Maslin, M., Viela, C., Mikkelsen, N., Grootes, P., 2005. Causes of catastrophic sediment failures of the Amazon Fan. Quaternary Science Reviews 24, 2180-2193.

McCorkle, D.C., Keigwin, L.D., Corliss, B.H., Emerson, S. R., 1990. The influence of microhabitats on the carbon isotopic composition of deep-sea benthic foraminifera. Paleoceanography 5, 161–185.

McGuire, A. D., Anderson, L.G., Christensen, T. R., Dallimore, S., Guo, L., Hayes, D.J., Heimann, M., Lorenson, T. D., MacDonald, R. W., Roulet, N., 2009. Sensitivity of the carbon cycle in the Arctic to climate change, Ecol. Monogr., 79(4), 523-555, doi:10.1890/08-2025.1.

Murray, J.W., 2006. Ecology and applications of benthic foraminifera, Cambridge University Press.

Naehr, T.H., Eichhubl, P., Orphan, V.J., Hovland, M., Paull, C.K., Ussler, W. III, Lorenson, T.D., Green, H.G., 2007. Authigenic carbonate formation at hydrocarbon seeps in continental margin sediments: a comparative study. Deep Sea Research Part II: Topical Studies in Oceanography, 54, 1268-1291.

Naehr, T.H., Birgel, D., Bohrmann, G., MacDonald, I.R., Kasten, S., 2009. Chemical Geology 266, 390-402. Biogeochemical controls on authigenic carbonate formation at the Chapopote "asphalt volcano", Bay of Campeche. https://doi.org/10.1016/j.chemgeo.2009.07.002.

O'Neil, J.R. and Epstein, S., 1966. Oxygen Isotope Fractionation in the System Dolomite-Calcite-Carbon Dioxide. Science 152, 198-201. DOI: 10.1126/science.152.3719.198.

Orphan W.G., Ussler W. III, Naehr, T.H., House, C.H., Hinrichs, K.-U., Paull, C.K., 2004. Geological, geochemical, and microbiological heterogeneity of the seafloor around methane vents in the Eel River Basin, offshore California, Chemical geology 205, 265-289.

Panieri, G., 2006. Foraminiferal response to an active methane seep environment: A case study from the Adriatic Sea. Marine Micropaleontology. 61, 116–130. http://dx.doi.org/10.1016/j.marmicro.2006.05.008.

Panieri, G., Camerlenghi, A., Conti, S., Pini, G.A., Cacho, I., 2009. Methane seepages recorded in benthic foraminifera from Miocene seep carbonates,Northern Apennines (Italy). Palaeogeography, Palaeoclimatology, Palaeoecology 284, 271-282.

Panieri, G., Camerlenghi, A., Cacho, I., Sanchez Cervera, C., Canals, M., Lafuerza, S., Herrera, G., 2012. Tracing seafloor methane emissions with benthic foraminifera: Results from the Anasubmarine landslide (Eivissa Channel, Western Mediterranean Sea). Marine Geology 291-294, 97-112.

Panieri, G., James, R.H., Camerlenghi, A., Cesari, V., Cervera, C.S., Cacho, I., Westbrook, G.K., 2014. Record of methane emissions from the West Svalbard continental margin during the last 16,000 years revealed by $\delta^{13}C$ of benthic foraminifera. Global and Planetary Change 122, 151–160. http://dx.doi.org/10.1016/j.gloplacha.2014.08.014.

Panieri, G., Graves, C.A., James, R.H., 2016. Paleo-methane emissions recorded in foraminifera near the landward limit of the gas hydrate stability zone off-shore western Svalbard. Geochemistry, Geophysics, Geosystem 17 (2), 521–537. http://dx.doi.org/10.1002/2015GC006153.

Panieri, G., Bünz, S., Fornari, D.J., Escartin, J., Serov. P., Jansson, P., Torres, M.E., Johnson, J.E., Hong, W.L., Sauer, S., Garcia, R., Gracias, N., 2017a. An integrated view of the methane

system in the pockmarks at Vestnesa Ridge, 79°N. Marine Geology 390, 282-300. http://dx.doi.org/10.1016/j.margeo.2017.06.006.

Panieri, G., Lepland, A., Whitehouse, M.J., Wirth, R., Raanes, M.P., James, R.H., Graves, C.A., Crémière, A., Schneider, A., 2017b. Diagenetic Mg-calcite overgrowths on foraminiferal tests in the vicinity of methane seeps. Earth and Planetary Science Letters 458, 203-212. http://dx.doi.org/10.1016/j.epsl.2016.10.024.

Petersen, C.J., Bünz, S., Hustoft, S., Mienert, J., Klaeschen, D., 2010. High-resolution P-Cable 3D seismic imaging of gas chimney structures in gas hydrated sediments of an Arctic sediment drift. Marine Petroleum Geology 27, 1981–1994. http://dx.doi.org/10.1016/j.marpetgeo.2010.06.006.

Pierre, C., Rouchy, J.-M., Blanc-Valleron, M.M., 2002. Gas hydrate dissociation in the Lorca Basin (SE Spain) during the Mediterranean Messinian salinity crisis. Sedimentary Geology 147, 247-252. https://doi.org/10.1016/S0037-0738(01)00232-9.

Racine, C., Bonnin, J., Nam, S.-I., Giraudeau, J., Biguenet, M., Dessandier, P.-A., Kim, J.-H., 2018. Distribution of living benthic foraminifera in the northern Chukchi Sea. Arktos 4: 28. https://doi.org/10.1007/s41063-018-0062-y

Rasmussen, T.L., Thomsen, E., Slubowska, M.A., Jessen, S., Solheim, A., Koc, N., 2007. Paleoceanographic evolution of the SW Svalbard margin (76°N) since 20,000 ^{14}C yr BP. Quaternary Research 67, 100–114.

Rathburn, A.E., Perez, E.M., Martin, J.B., Day, S.A., Mahn, C., Gieskes, J., Ziebis, W., Williams, D., Bahls, A., 2003. Relationships between the distribution and stable isotopic composition of living benthic foraminifera and cold methane seep biogeochemistry in Monterey Bay, California. Geochemistry, Geophysics, Geosystem 4. http://dx.doi.org/10.1029/2003GC000595.

Ravelo, A. C., and Hillaire Marcel, C., 1999. The Use of Oxygen and Carbon Isotopes of Foraminifera in Paleoceanography. In Proxies in Late Cenozoic Paleoceanography. Developments in Marine Geology 1, 735-760.

Rise, L., Bøe, R., Riis, F., Bellec, V.K., Laberg, J.S., Eidvin, T., Elvenes, S., and Thorsnes, T., 2013. The Lofoten-Vesterålen continental margin, North Norway: canyons and mass-movement activity, Marine and Petroleum Geology, 45, 134-149.

Roberts, H.H. and Aharon, P., 1994. Hydrocarbon-derived carbonate buildups of the northern Gulf of Mexico continental slope: A review of submersible investigations. Geo-Marine Letters 14, 135-148.

Sauer, S., Hong, W.-L., Knies, J., Lepland, A., Forwick, M., Klug, M., Eichinger, F., Baranwal, S., Crémière, A., Chand, S. and Schubert, C.J. (2016) Sources and turnover of organic carbon and methane in fjord and shelf sediments off northern Norway. Geochemistry, Geophysics, Geosystems 17, 4011-4031.

Sauer, S., Crémière, A., Knies, J., Lepland, A., Sahy, D., Martma, T., Noble, S.R., Schönenberger, J., Klug, M. and Schubert, C.J., 2017. U-Th chronology and formation controls of methane-derived authigenic carbonates from the Hola trough seep area, northern Norway. Chemical Geology 470, 164-179.

Schönfeld, J., Alve, E., Geslin, E., Jorissen, F., Korsun, S., Spezzaferri, S., 2012. The FOBIMO (FOraminiferal BIo-MOnitoring) initiative—Towards a standardized protocol for soft-bottom benthic foraminiferal monitoring studies. Marine Micropaleontology 94-95, 1-13.

Schneider, A., Crémière, A., Panieri, G., Lepland, A., Knies, J., 2017. Diagenetic alteration of benthic foraminifera from a methane seep site on Vestnesa Ridge (NW Svalbard). Deep-Sea Research I 123, 22-34. http://dx.doi.org/10.1016/j.dsr.2017.03.001.

Schneider, A., Panieri, G., Lepland, A., Consolaro, C., Crèmiére, A., Forwick, M., Johnson, J.E., Plaza-Faverola, A., Sauer, S., Knies, J., 2018. Diagenetically altered benthic foraminifera reveal paleo-methane seepage. Quaternary Science Reviews 193, 98-117.

Schroeder, J.O., Murray, R.W., Leinen, M., Pflaum, R.C., Janecek, T.R., 1997. Barium in equatorial Pacific carbonate sediment: Terrigenous, oxide, and biogenic association. Paleoceanography 12, 125-146.

Schumacher, S., Jorissen, F., Mackensen, A., Gooday, A.I., Pays, O., 2010. Ontogenetic effects on stable carbon and oxygen isotopes in tests of live (Rose Bengal stained) benthic foraminifera from the Pakistan continental margin. Marine Micropaleontology 76, 92-103.

Screen, J.A., and Simmonds, I., 2010. The central role of diminishing sea ice in recent Arctic temperature amplification. Nature 464, 1334-1337.

Sen, A., Himmler, T., Hong, W.-L., Chitkara, C., Lee, R.W., Ferré, B., Lepland, A., Knies, J., 2019. Atypical biological features of a new cold seep site on the Lofoten-Vesterålen continental margin (northern Norway). Scientific Reports 9: 1762. https://doi.org/10.1038/s41598-018-38070-9

Sen Gupta, B.K., Aharon, P., 1994. Benthic foraminifera of bathyal hydrocarbon vents of the Gulf of Mexico: initial report on communities and stable isotopes. Geo-Marine Letters 14, 88–96.

Serov, P., Vadakkepuliyambattaa, S., Mienert, J., Patton, H., Portnov, A., Silyakova, A., Panieri, G., Carroll, M.L., Carroll, J., Andreassen, K., Hubbard, A., 2017. Postglacial response of Arctic Ocean gas hydrates to climatic amelioration. Proceedings of the National Academy of Sciences of the United States of America 114, 6215-6220.

Serreze, M.C. and Barry, R.G., 2011. Processes and impacts of Arctic amplification: A research synthesis. Global and Planetary Change 77, 85-96.

Sloan, E.D. Jr., Koh, C., 2007. Clathrate hydrates of natural gases, 3rd ed. CRC Press.

Spero, H.J., Bijma, J., Lea, D.W., Bemis, B. E., 1997. Effect of seawater carbonate concentration on foraminiferal carbon and oxygen isotopes. Nature 390, 497-500.

Steinle, L., Graves, C.A., Treude, T., Ferre, B., Biastoch, A., Bussmann, I., Berndt, C., Krastel, S., James, R.H., Behrens, E., Böning, C.W., Greinert, J., Sapart, C.-J., Schreinert, M., Sommer, S., Lehmann, M.F., Niemann, H., 2015. Water column methanotrophy controlled by a rapid oceanographic switch. Nature Geoscience 8, 378–382.

Tagliabue, A., Bopp., L., 2008. Towards understanding global variability in ocean carbon-13. Gloobal Biogeochemical Cycles 22, GB1025. doi:10.1029/2007GB003037.

Talwani, M. and Eldholm, O., 1977, Evolution of the Norwegian-Greenland Sea: Geological Society of America Bulletin 88, 969–999. doi: 10.1130 /0016-606(1977)88<969:EOTNS>2.0.CO;2.

Tarutani, T., Clayton, R.N., Mayeda, T.K., 1969. The effect of polymorphism and magnesium substitution on oxygen isotope fractionation between calcium carbonate and water. Geochimica et Cosmochimica Acta 33, 987-996. https://doi.org/10.1016/0016-7037(69)90108-2.

Thatcher, K.E., Westbrook, G.K., Sarkar, S., Minshull, T.A., 2013. Methane release from warming-induced hydrate dissociation in the West Svalbard continental margin: Timing, rates, and geological controls. Journal of Geophysical Research: Solid Earth 118, 22-38.

Thiede, J., Winkler, A., Wolf-Welling, T., Eldholm, O., Myhre, A.M., Baumann, K.H., Henrich, R., Stein, R., 1998. Late Cenozoic history of the Polar North Atlantic: results from ocean drilling. Quaternary Science Reviews 17, 185–208.

Thomas, D.J., Zachos, J.C., Bralower, T.J., Thomas, E., Bohaty, S., 2002. Warming the fuel for the fire: Evidence for the thermal dissociation of methane hydrate during the Paleocene-Eocene thermal maximum. Geology 30, 1067-1070.

Tomaru, H., Torres, M.E., Matsumoto, R., and Borowski, W.S., 2006. Effect of massive gas hydrate formation on the water isotopic fractionation of the gas hydrate system at Hydrate Ridge, Cascadia margin, offshore Oregon. Geochemistry Geophysics Geosystems, 7, Q1000110.1029/2005gc001207,.

Torres, M.E., Mix, A.C., Kinports, K., Haley, B., Klinkhammer, G. P, McManus, J., de Angelis, M. A., 2003. Is methane venting at the seafloor recorded by δ13C of benthic foraminifera shells? Paleoceanography, 18 (3), 1062, doi:10.1029/2002PA000824.

Torres, M. E., Mix, A. C., and Rugh, W. D., 2005. Precise delta C-13 analysis of dissolved inorganic carbon in natural waters using automated headspace sampling and continuous-flow mass spectrometry. Limnology and Oceanography-Methods 3, 349-360.

Ussler, W., Paull, C.K., 2008. Rates of anaerobic oxidation of methane and authigenic carbonate mineralization in methane-rich deep-sea sediments inferred from models and geochemical profiles. Earth and Planetary Science Letters 266, 271-287.

Vasconcelos, C., McKenzie, J.A., Warthmann, R. and Bernasconi, S.M., 2005. Calibration of the $\delta^{18}O$ paleothermometer for dolomite precipitated in microbial cultures and natural environments. Geology 33.

Vogt, P.R., Crane, K., Sundvor, E., Max, M.D., Pfirman, S.L., 1994. Methane-generated (?) pockmarks on young, thickly sedimented oceanic crust in the Arctic: Vestnesa Ridge, Fram Strait. Geology 22, 255-258.

Walton, W.R., 1952. Techniques for recognition of living foraminifera. In: Contribution of the Cushman Foundation for Foraminiferal Research. 3. pp. 56–60.

Wan, S., Feng, D., Chen, F., Zhuang, C., Chen, D., 2018. Foraminifera from gas hydrate-bearing sediments of the northeastern South China Sea: Proxy evaluation and application for methane release activity. Journal of Asian Earth Sciences 168, 125-136.

Wefer, G., Heinze, P.-M., Berger, W.H., 1994. Clues to ancient methane release. Nature 369, 282.

Whiticar, M.J., 1999. Carbon and hydrogen isotope systematics of bacterial formation and oxidation of methane. Chemical Geology 161, 291-314.

Yao, H., Hong, W.-L., Panieri, G., Sauer, S., Torres. M.E., F. Lehmann, M.F., Gründger, F., Niemann, H., 2019. Fracture-controlled fluid transport supports microbial methane-oxidizing communities at the Vestnesa Ridge. Biogeosciences 16, 2221-2232.

Yoshinaga, M. Y., Holler, T., Goldhammer, T., Wegener, G., Pohlman, J. W., Brunner, B., Kuypers, M. M., Hinrichs, K.-U., and Elvert, M., 2014. Carbon isotope equilibration during sulphate-limited anaerobic oxidation of methane, Nature Geoscience, 7, 190.

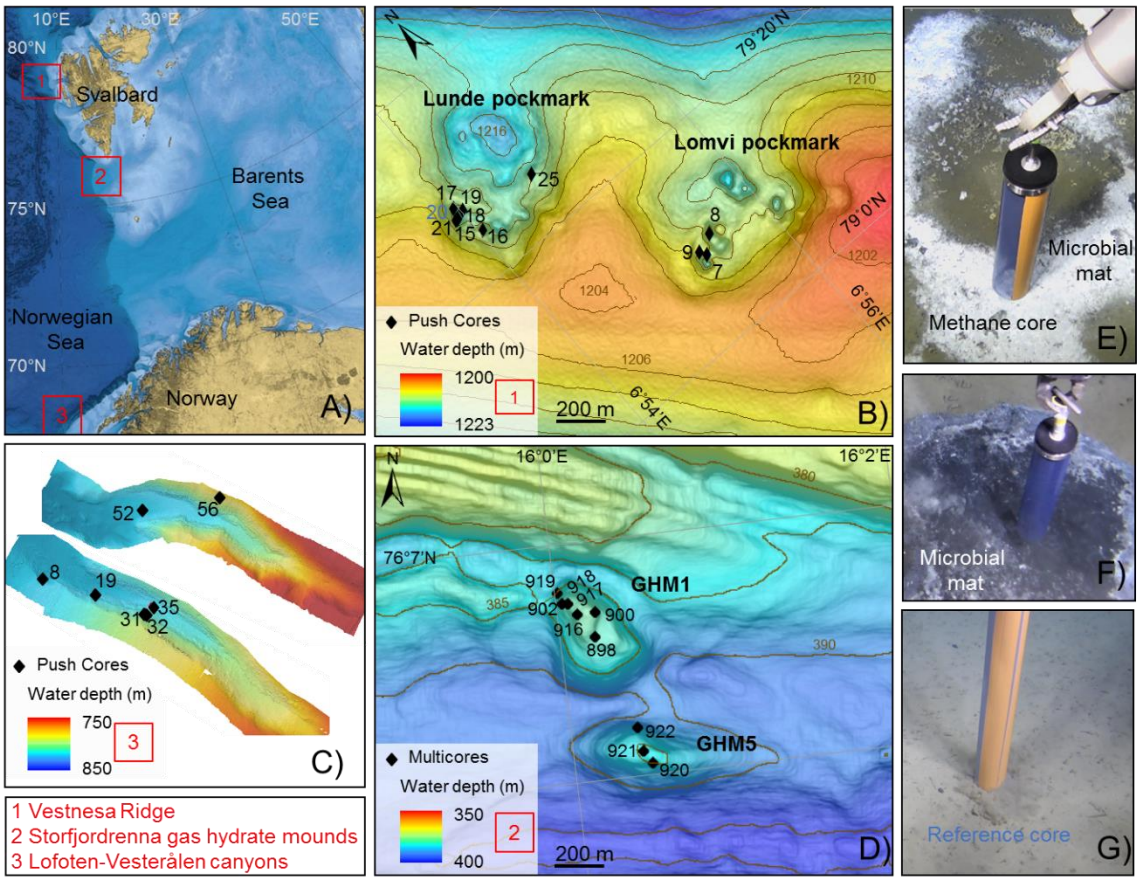

Figure 1. A) Map of the study area with sample areas identified by red squares. B) Location of the push cores collected within two pockmarks (Lunde and Lomvi) on Vestnesa Ridge. C) Location of push cores collected within the Lofoten-Vesterålen canyon region (Canyons North and South). D) Location of multicores collected in Storfjordrenna (GHMs 1 and 5). E) and F) Examples of push cores collected on microbial mats covering methane-rich sediments (i.e., cores V-8 and V-16, respectively) and G) Example of a push core collected outside a microbial mat (i.e., core V-20).

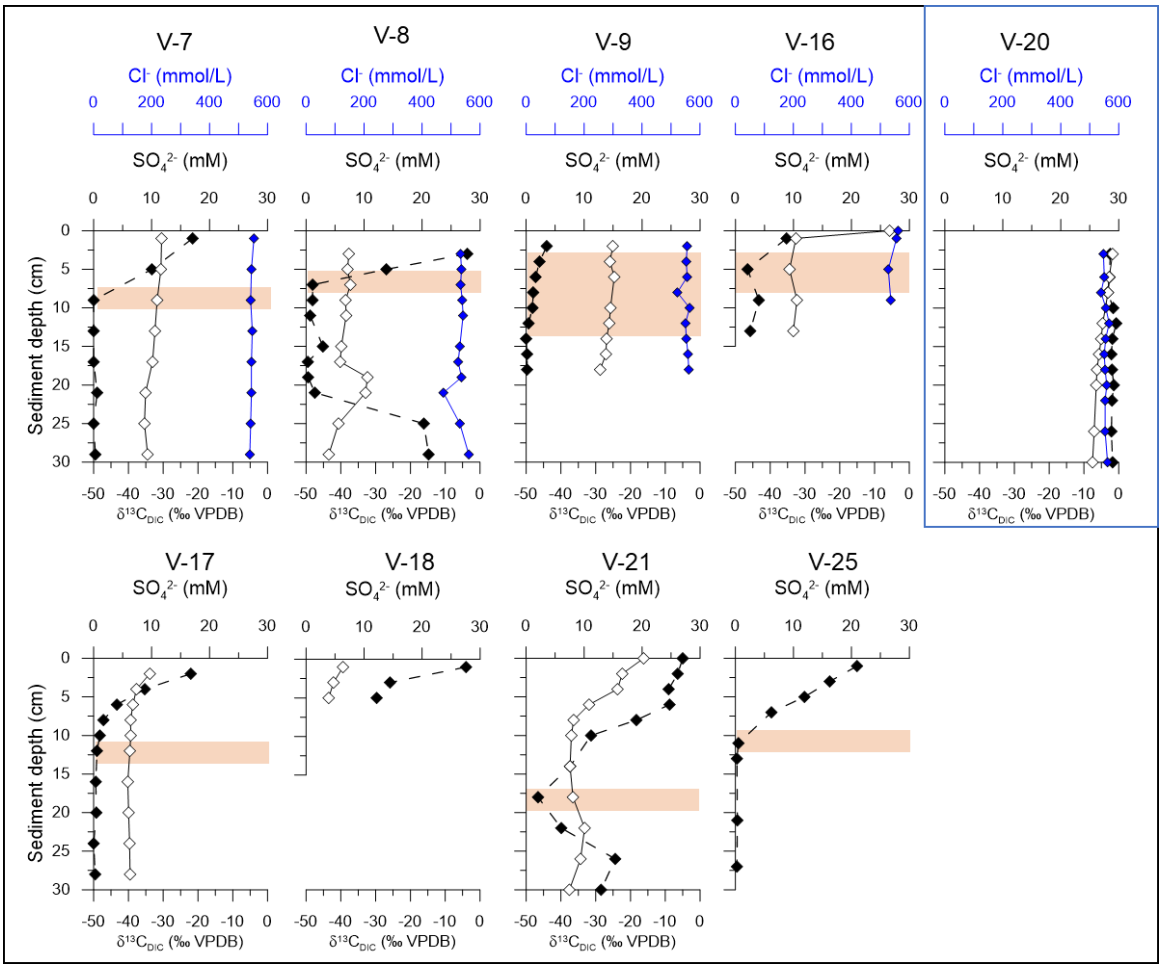

Figure 2. Pore water sulfate (SO_4^{2-}, black), $\delta^{13}C_{DIC}$ (white), and Chloride (Cl^-, blue) profiles of push cores collected at Vestnesa Ridge. The numbers at the top of each graph identify the stations; the blue square indicates the core sampled outside a microbial mat (control core). The estimated sulfate-methane transition is in orange.

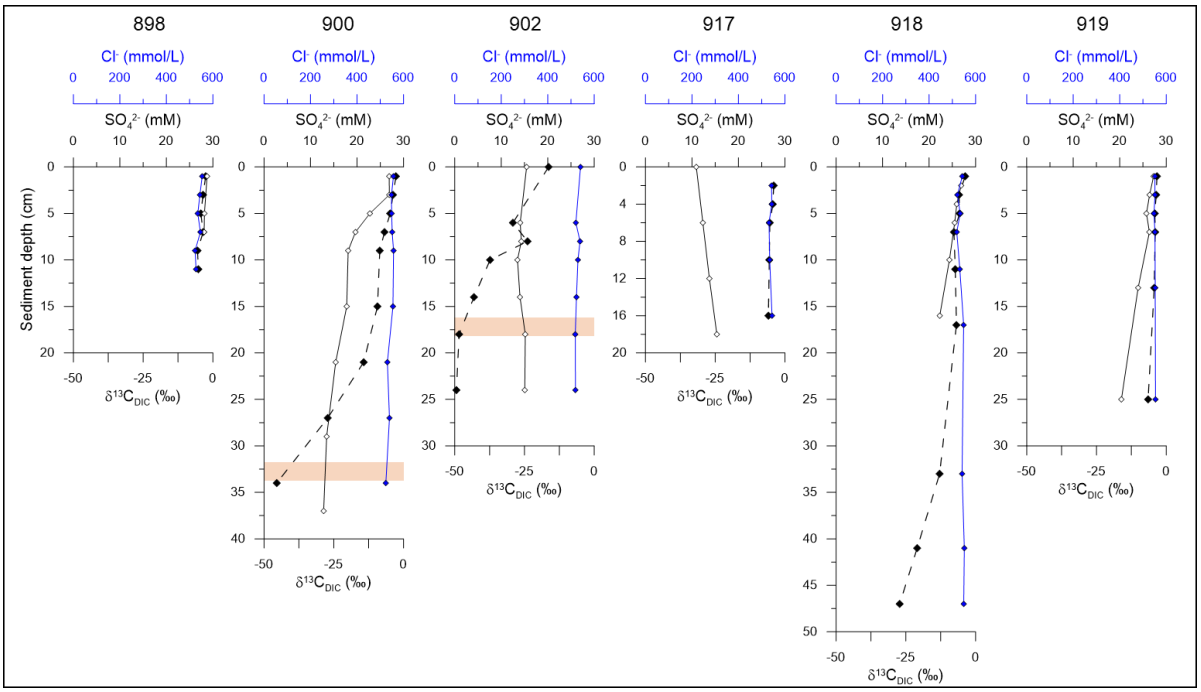

Figure 3. Pore water sulfate (SO_4^{2-}, black), $\delta^{13}C_{DIC}$ (white), and Chloride (Cl^-, blue) profiles of multicores collected at Storfjordrenna GHM1. The numbers at the top of each graph identify the stations; the estimated sulfate-methane transition is in orange.

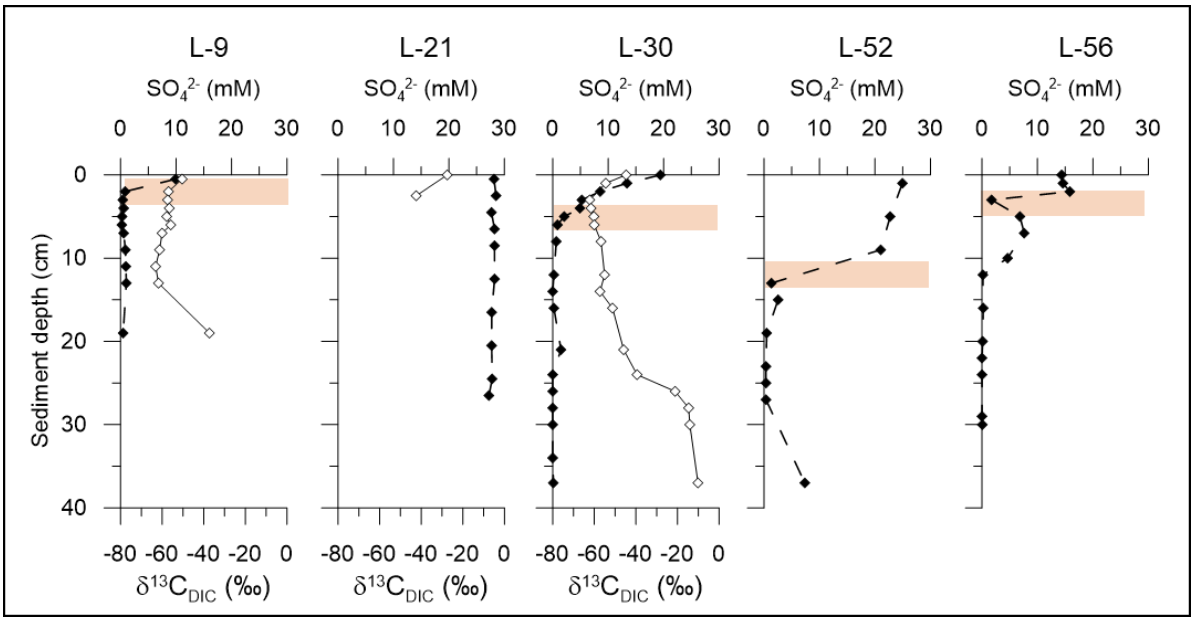

Figure 4. Pore water sulfate (SO_4^{2-}, black) and $\delta^{13}C_{DIC}$ (white) profiles of push cores collected at the Lofoten-Vesterålen canyons. The numbers at the top of each graph identify the stations; the estimated sulfate-methane transition is in orange.

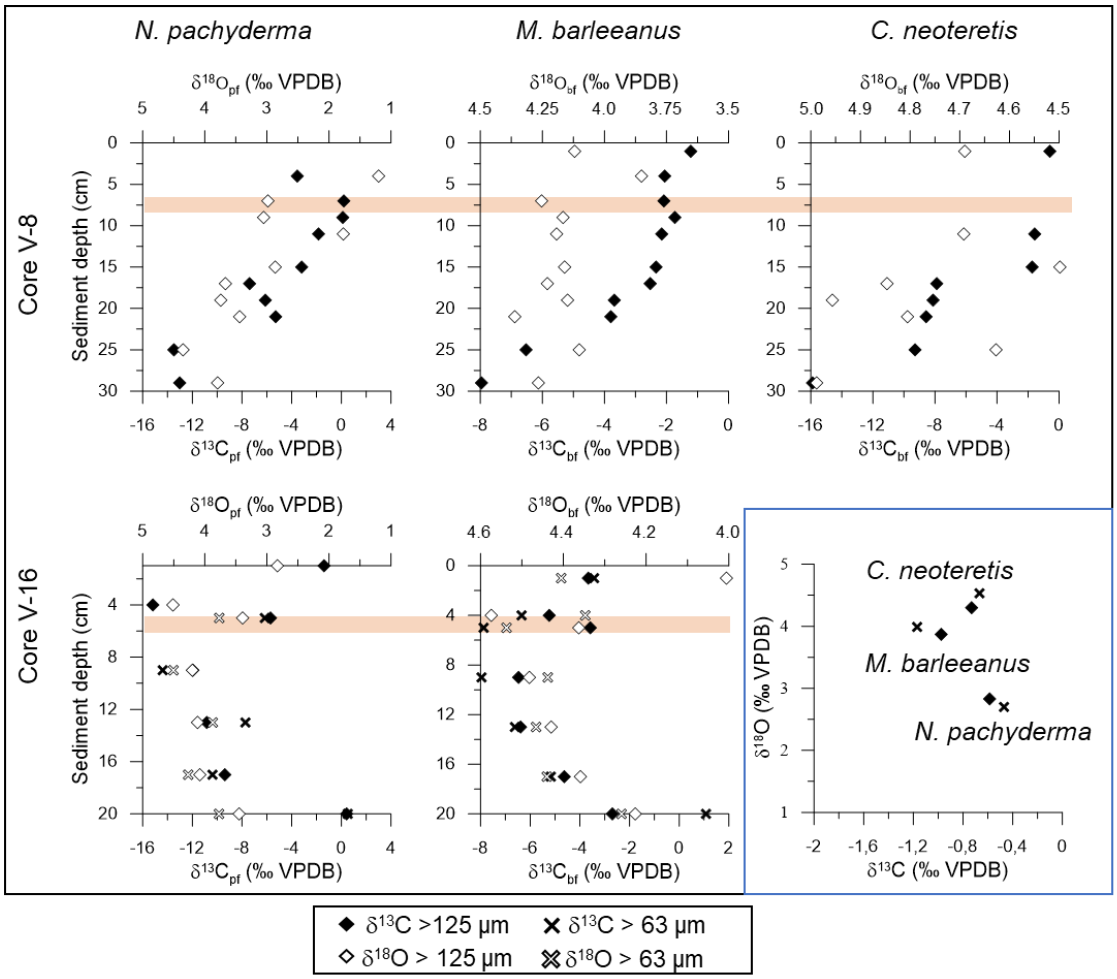

Figure 5. Cores V-8 and V-16 (Vestnesa Ridge) planktonic (pf) and benthic (bf) foraminiferal isotopes ($\delta^{13}C$ and $\delta^{18}O$) data. The blue square indicates the values measured on the surface sample (0-1 cm) of core V-20. Analyses were performed on two benthic (*C. neoteretis* and *M. barleeanus*) and one planktonic (*N. pachyderma*) foraminiferal species. Diamonds are used to identify data collected analyzing the fraction >125 µm. Crosses are used to identify data collected analyzing the fraction >63 µm. VPDB = Vienna Pee Dee Belemnite.

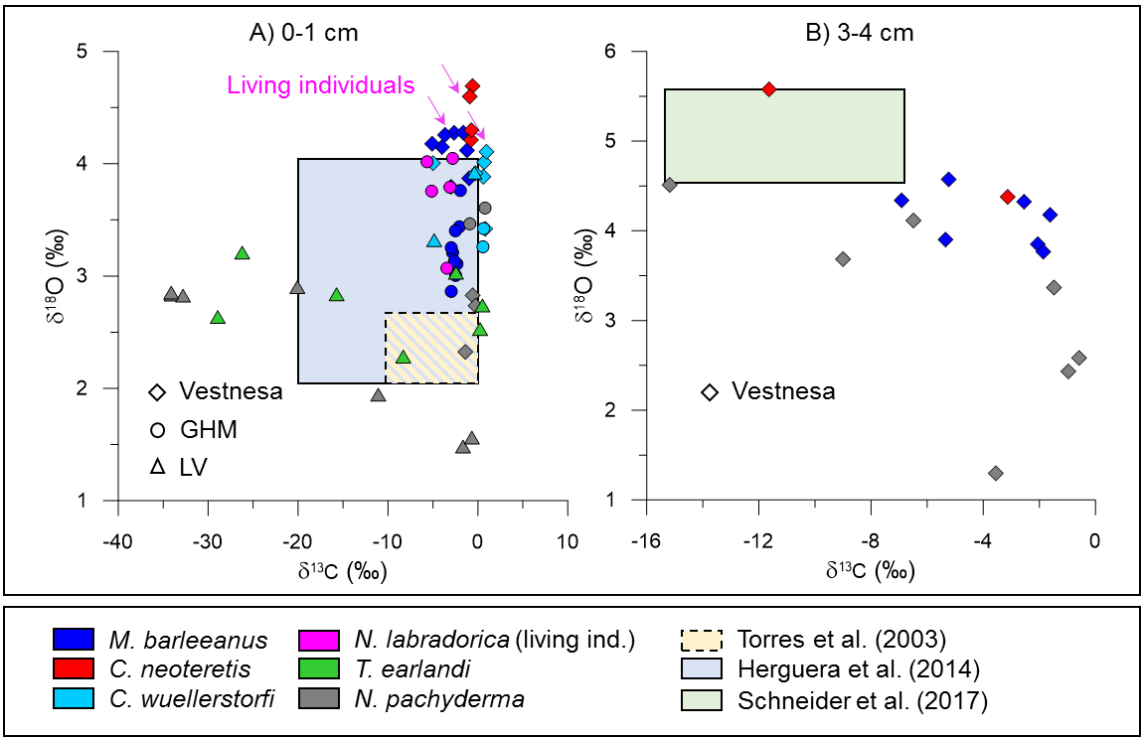

Figure 6. Foraminiferal stable isotopes ($\delta^{13}C$ and $\delta^{18}O$) measured on benthic (colored symbols) and planktonic (grey symbols) species. A) Data collected from surface samples (0-1 cm) of cores from Vestnesa Ridge, Storfjordrenna (GHM), and the Lofoten-Vesterålen Canyons. Data from Rose Bengal stained ('living') individuals are identified by pink arrows. B) Data collected from the interval 3-4 cm of cores collected at Vestnesa Ridge. Colored areas in (A) show the range of isotopic values of benthic foraminifera from methane seeps and gas hydrate-rich sediments from different geographic locations (Hydrate Ridge (in yellow) and Gulf of California (in blue); Torres et al., 2003, Herguera et al., 2014). All the foraminifera analyzed were picked from superficial sediments (0-5 cm) and were affected by secondary overgrowth. The green square in panel (B) shows the range of values measured on benthic foraminifera from Vestnesa Ridge (Schneider et al., 2017). The foraminifera analyzed were picked deeper in the sediment column (meters below the seafloor) and were affected by secondary overgrowth. VPDB = Vienna Pee Dee Belemnite.

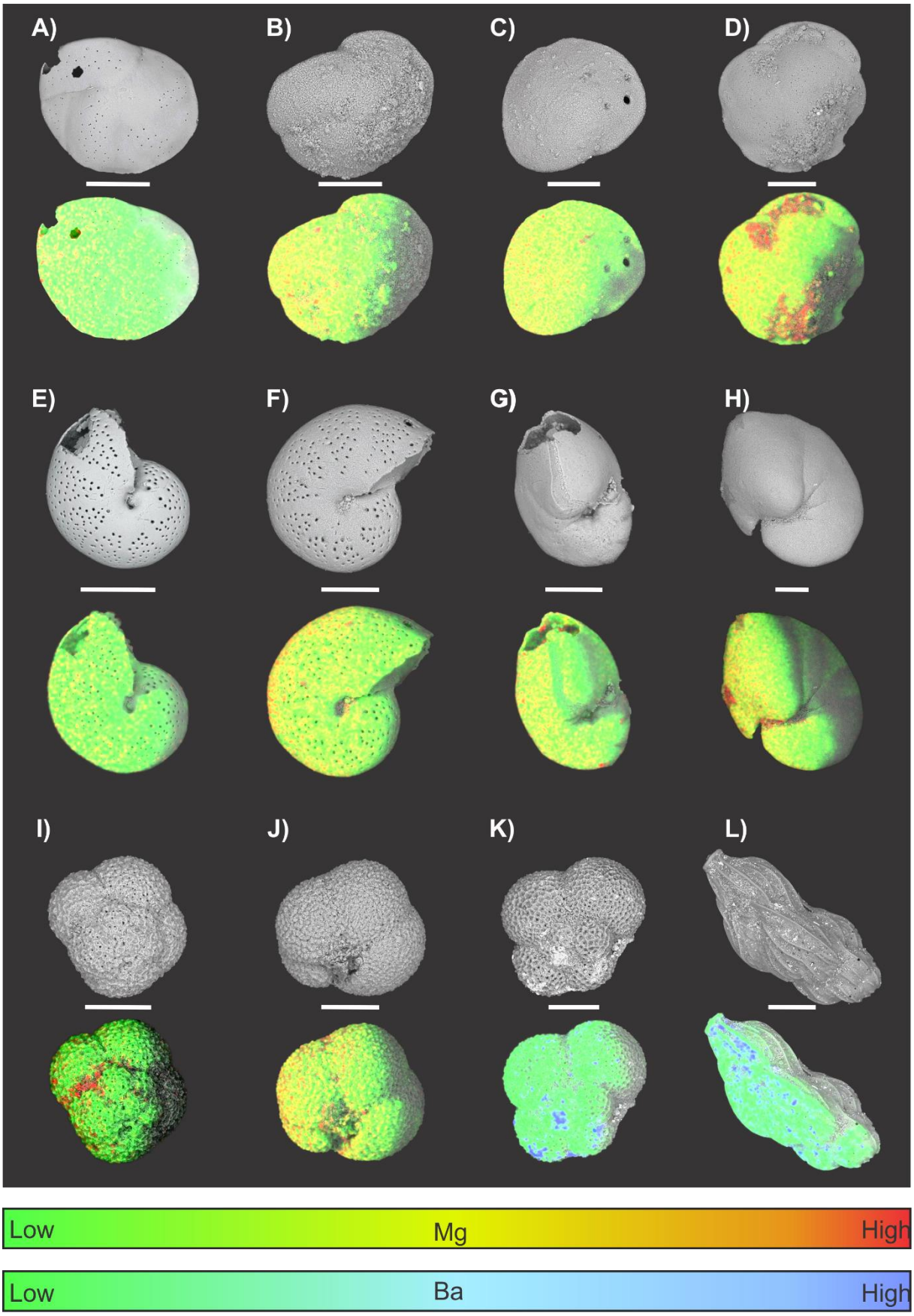

Figure 7. Backscatter-scanning electron microscopy images and corresponding energy-dispersive x-ray spectroscopy (EDS) maps of selected foraminiferal shells. *Cassidulina*

neoteretis from core V-16 0-1 cm (A) and 3-4 cm (B), and core V-8, 3-4 cm (C) and 29-30 cm (D). *Melonis barleeanus* from core GHM1 0-1 cm (Rose Bengal stained specimen) (E), and core V-8 29-30 cm (F). *Nonionella labradorica* from core GHM1 0-1 cm (Rose Bengal stained specimen) (G), and core V-8 29-30 cm (H). *Neogloboquadrina pachyderma* from core V-8 0-1 cm (I), core V-8 29-30 cm (J), and core L-8 0-1 cm (K). *Trifarina earlandi* from Lofoten-Vesterålen L-19 0-1 cm (L). Scale bars are 100 µm. Grey areas on EDS maps represent portions of the shells where the analysis was not possible, due to the angle of the detector and shell morphology.

Table 1. Summary of the cores collected at Vestnesa Ridge (Lomvi and Lunde), Storfjordrenna (GHMs 1 and 5), and the Lofoten-Vesterålen canyons (Canyons South and North) and used in this study. The analyses performed on each core are specified. Chloride data are not available for the LV Canyons cores. The data collected are reported in Supplementary Tables 1, 2 and 3. Nd = no data.

Core reference	name	Location	latitude ˚N	longitude ˚E	water depth (m)	pore water SO_4^{2-}, $\delta^{13}C_{DIC}$, Cl^- (cm)	foraminifera stable isotopes (cm)
P1606-007	V-7	Lomvi	79.0023	6.225	1204	0-30	0-5
P1606-008	V-8	Lomvi	79.0027	6.9248	1208	0-30	0-30
P1606-009	V-9	Lomvi	79.0025	6.922	1205	0-20	0-5
P1606-015	V-15	Lunde	79.0076	6.9003	1208	0-30	0-2
P1606-016	V-16	Lunde	79.0068	6.9006	1206	0-15	0-20
P1606-017	V-17	Lunde	79.0078	6.8994	1205	0-30	0-5
P1606-018	V-18	Lunde	79.0075	6.899	1207	0-7	0-5
P1606-019	V-19	Lunde	79.0075	6.8986	1207	nd	0-5
P1606-020	V-20	Lunde	79.0075	6.899	1207	0-30	0-1
P1606-021	V-21	Lunde	79.0075	6.8989	1207	0-30	0-5
P1606-025	V-25	Lunde	79.0071	6.9111	1200	0-30	0-5
P1702-898	898	GHM1	76.1144	16.0033	380	0-12	0-1
P1702-900	900	GHM1	76.1150	16.0036	380	0-35	0-1
P1702-902	902	GHM1	76.1153	16.0011	377	0-25	0-1
P1702-916	916	GHM1	76.1150	16.0019	377	nd	0-1
P1702-917	917	GHM1	76.1153	16.0011	377	0-20	0-1
P1702-918	918	GHM1	76.1153	16.0006	389	0-50	0-1
P1702-919	919	GHM1	76.1156	16.0003	378	0-25	0-1
P1702-920	920	GHM5	76.1114	16.0075	379	nd	0-1
P1702-921	921	GHM5	76.1117	16.0067	380	nd	0-1
P1702-922	922	GHM5	76.1122	16.0064	386	nd	0-1
P1710-008	L-8	Canyon South	68.1583	10.4607	794	nd	0-1
P1710-009	L-9	Canyon South	68.1583	10.4606	794	0-20	nd
P1710-012	L-12	Canyon South	68.1591	10.4559	804	0-30	nd
P1710-019	L-19	Canyon South	68.1587	10.4561	794	nd	0-1
P1710-030	L-30	Canyon South	68.1578	10.4654	770	0-40	nd
P1710-031	L-31	Canyon South	68.1578	10.4653	769	nd	0-1
P1710-032	L-32	Canyon South	68.1578	10.4654	769	nd	0-1
P1710-035	L-35	Canyon South	68.158	10.4658	778	nd	0-1
P1710-052	L-52	Canyon North	68.1665	10.4633	807	0-40	0-1
P1710-056	L-56	Canyon North	68.1671	10.4702	782	0-30	0-1